AD NUMBER
AD914312
LIMITATION CHANGES
TO: **Approved for public release; distribution is unlimited.**
FROM: **Distribution authorized to U.S. Gov't. agencies only; Test and Evaluation; 23 JAN 1973. Other requests shall be referred to Army Advanced Ballistic Missile Defense Agency, Huntsville, AL 35807.**
AUTHORITY
ABMDA ltr 4 Feb 1974

RDA-TR-2403-003

FINAL REPORT ON MIDCOURSE AREA DEFENSE CONCEPTS
VOLUME III - SYSTEM CONFIGURATION AND FEASIBILITY OF AN X-RAY SENSOR FOR EXO-ATMOSPHERIC USE

AUGUST 1973

By:
. SANBORN

Sponsored By:
ADVANCED BALLISTIC MISSILE DEFENSE AGENCY

R & D ASSOCIATES
Post Office Box 3580
Santa Monica,
California, 90403

525 WILSHIRE BOULEVARD • SANTA MONICA • TELEPHONE: (213) 451-5838

REPORT DOCUMENTATION PAGE

READ INSTRUCTIONS BEFORE COMPLETING FORM

1. REPORT NUMBER: RDA-TR-2403-003	2. GOVT ACCESSION NO.
3. RECIPIENT'S CATALOG NUMBER	
4. TITLE (and Subtitle): FINAL REPORT ON MIDCOURSE DEFENSE CONCEPTS VOLUME III. SYSTEM CONFIGURATION AND FEASIBILITY OF AN X-RAY SENSOR FOR EXO-ATMOSPHERIC USE	5. TYPE OF REPORT & PERIOD COVERED: Final Technical Report 15 March 73 - 30 June 73
	6. PERFORMING ORG. REPORT NUMBER
7. AUTHOR(s): J. Sanborn	8. CONTRACT OR GRANT NUMBER(s): DAHC60-72-C-0123 MOD P00004
9. PERFORMING ORGANIZATION NAME AND ADDRESS: R & D Associates, P.O. Box 3580, Santa Monica, California 90403	10. PROGRAM ELEMENT, PROJECT, TASK AREA & WORK UNIT NUMBERS
11. CONTROLLING OFFICE NAME AND ADDRESS: U.S. Army SAFEGUARD System Command, Contracts Office, SSC-CS, P.O. Box 1500, Huntsville, Alabama 35807	12. REPORT DATE: August 1973
	13. NUMBER OF PAGES: 78
14. MONITORING AGENCY NAME & ADDRESS (if different from Controlling Office): Director, Advanced Ballistic Missile Defense Agency, P.O. Box 1500, Huntsville, Alabama 35807	15. SECURITY CLASS. (of this report): UNCLASSIFIED
	15a. DECLASSIFICATION/DOWNGRADING SCHEDULE: N/A

16. DISTRIBUTION STATEMENT (of this Report)

Distribution limited to U.S. Government Agencies only; Test and Evaluation; 23 January 1973. Requests by other agencies should be addressed to the Director, U.S. Army Advanced Ballistic Missile Defense Agency, Huntsville Office, Attn: RDMH-S, P.O. Box 1500, Huntsville, Alabama 35807.

17. DISTRIBUTION STATEMENT (of the abstract entered in Block 20, if different from Report)

18. SUPPLEMENTARY NOTES

19. KEY WORDS (Continue on reverse side if necessary and identify by block number)

20. ABSTRACT (Continue on reverse side if necessary and identify by block number)

The feasibility of exo-atmospheric discrimination of replica balloon decoys from reentry vehicles by means of an X-ray sensor system in a Midcourse Defense (MCD) context is analyzed. The discrimination relies on the fact that a replica decoy will contain less electrons than a reentry vehicle (RV) and thus if these objects are subjected to a flux of high energy X-rays, the Compton scattered radiation will be at least an order of magnitude greater for the RV. A first-order analysis and modeling of the system is performed, and the resulting expected performance is presented. Due to the characteristic distance and time parameters imposed by the MCD context, it is found to be unfeasible at the present time.

TABLE OF CONTENTS

LIST OF FIGURES

LIST OF TABLES

1. THE FEASIBILITY OF X-RAY DISCRIMINATION OF BALLOON REPLICA DECOYS

Advanced postulated MCD threats [1] include so called replica decoy balloons. These inflatable exoatmospheric decoys are designed to have virtually the same radar and infrared signatures as the true reentry vehicle. Replicas of this sort have been constructed and test flown by Lincoln Labs [2]. Unconventional (non-radar and non-IR) means for exo-discrimination are needed to counter this threat.

One such approach for discriminating replica decoys (RD's) involves the possibility of "taking an X-ray picture" of a potential decoy to "see" what is inside it. The intuitive basis for this concept is that energetic X-rays having great penetrating capabilities will probe the inners of the object being viewed and the scattered radiation will be highly dependent on the amount of matter inside. Since the decoy has very little content compared to the RV, we expect a different X-ray signature.

We can picture the geometry of the system as shown in Figure 1-1. An X-ray generating device which we will refer to as an X-ray transmitter at a distance R_T from the RV and RD's shines a spectrum of X-rays in the general direction of the objects to be discriminated. After the penetrating X-ray photons have entered these objects, some will be absorbed (photo-electric effect) and some scattered (Compton effect). The scattered X-ray radiation is then collected by an X-ray receiver at a distance R_R which has directionality characteristics fine enough to resolve the various objects. Note that the receiver and transmitter can be on the same or separate (space) platforms. The platforms cannot be operated in the lower atmosphere because of adverse absorption there.

We can immediately write down a "radar equation" [3] for the signal power P_R received at the X-ray receiver in terms of the X-ray transmitter power P_T as:

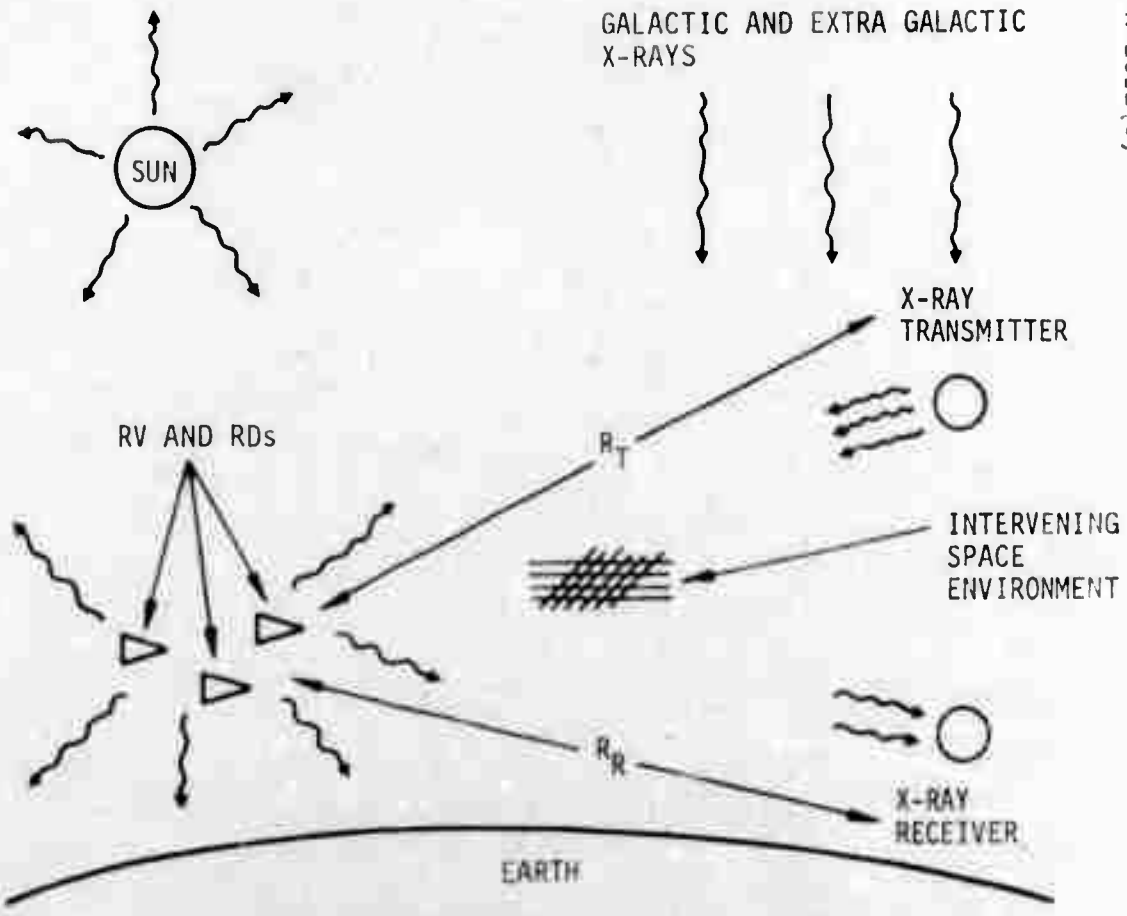

Figure 1-1(U). System Configuration

$$P_R = \left(\frac{P_T}{4\pi}\right) G_T \left(1-L_T\right) \left(\frac{\Sigma}{R_T^2}\right)\left(\frac{A_R}{R_R^2}\right) S \left(1-L_R\right) \qquad (1)$$

where G_T = gain in the transmitter, i.e., the ratio of power per steradian in the direction of the target to the isotropic power per steradian $P_T/4\pi$.

Σ = area of the target presented to the X-ray beam which will depend on orientation of the target.

A_R = effective area over which the receiver collects scattered X-rays.

S = ratio of the power scattered by the target per steradian in the direction of the receiver to the incident power. It will depend on the geometry of target, receiver and transmitter and on the chemical composition of the target.

L_T and L_R are fractional losses due to intervening environments between transmitter to target and target to receiver, respectively.

In order to appreciate the weakness of the received signal, we will consider the following order of magnitude quantities as typical (from the latter text of this report) for the case of the X-ray probe:

$G_T P_T \approx 10^{17}$ photons/second

note: we are using a number of photon interpretation of Equation (1) instead of power.

$$\Sigma \simeq 45 \text{ ft}^2$$

$$R_T \simeq R_R = 5 \times 10^4 \text{ ft (i.e., } \simeq \text{ nine miles)}$$

$$L_T = L_R = 0$$

$$S = \frac{1}{4\pi} \text{ (isotropic scattering of all impinging photons)}$$

Equation (1) then yields

$$P_{R/A_R} \simeq 5 \times 10^{-6} \text{ photons/cm}^2 \text{ sec} .$$

Leaving signal to noise considerations aside, the receiver must detect at least one photon in its allowed viewing time T_R, (i.e., $P_R > 1$ photon $/T_R$) in order to sense the presence of an X-ray scatterer. This implies the receiver must have a collection area A_R such that $A_R T_R > 2 \times 10^5$ cm^2 sec. As a nominal value assume $T_R \sim 1$ sec (to be rationalized later), then A_R must be greater than 10^5 cm^2, which is orders of magnitude more collection area than present day (hard) X-ray detectors.

An order of magnitude argument like that given above indicates that it is presently unfeasible to have a system which could act as an X-ray sensor at a range of nine miles. However, in order to judge the future feasibility, we must examin in detail the connection between the various parameters involved in the (a) X-ray generator, (b) target, and (c) the X-ray receiver. In the following we will model the various components of the system and consider the system synthesis of an X-ray direction finding sensor.

After this research was completed, it was realized that one significant aspect of signal to noise improvement was overlooked. This involves using a pulsed X-ray generator with a receiver adjusted to receive

scattered radiation only during the appropriate pulse reception times. For such a system, we can approach the limit of almost zero noise as illustrated above. We have, therefore, inserted a section on the qualitative features of a pulsed system.

At the end of the report, we will consider the potential for increasing gain (in transmitter or receiver) by means of focusing X-rays and the possibility of an X-ray laser.

2. THE X-RAY TRANSMITTER

The X-ray transmitter is simply an X-ray generating device. In general an X-ray generator consists of three parts:

1. A source of free electrons
2. An electron accelerator
3. A target

The high energy electron beam impinging on the target is decelerated abruptly with the resultant emission of radiation (Bremsstrahlung). We will not consider X-ray-emitting radioactive substances because of their low flux levels.

The source of free electrons is invariably a thermionic emitter commonly referred to as the cathode because it usually is at a higher potential than the rest of the apparatus. The cathode is heated by ohmic resistance to a very high temperature and a large voltage drop is applied between the cathode and "free space" to overcome the work function of the material and thus enhance thermionic emission of electrons.

Many different accelerator designs have been developed. In the lower energy regions (less than $\simeq$ 500 keV), the same potential drop which was used to enhance thermionic emission is used to accelerate the electrons. This is the conventional X-ray tube found in doctors' or dentists' offices. At moderate electron beam energies (500 keV $\sim$ 5 MeV), compact linear accelerators are used. These consist of a sequence of potential drops in series. Energies of around 1 MeV per foot have been achieved without spurious electrical discharge. In the high energy region (greater than $\sim$ 3 MeV) toroidal accelerators are used such as the betatron which confines the electron beam to a ring by magnetic fields and accelerates the beam by magnetic induction.

Roughly, the efficiency of conversion of electron beam energy to X-ray energy goes proportional to the atomic number Z of the target material. For this reason, high-Z materials are usually chosen. Because heating of the target is usually a problem, it is best to use a high melting temperature substance with as low vapor pressure as possible. Tungsten (Z = 74) is ideal for this purpose and we will assume a tungsten target for the analysis.

In Figure 2-1 we have a plot of beam energy versus average beam current for some typical X-ray devices. In general, the high energy electron beam devices are pulsed so we have used time averaged (over many pulses) currents. Each point is an X-ray generator. We have plotted the high power output devices mentioned in References 4 and 5. These references, however, are somewhat dated (greater than ten years). In the low electron energy regime, we have shown some industrial X-ray tube devices including some (few second rated) rotating anode devices. For moderate to high energies, we have plotted mostly pulsed devices ranging from Van de Graff generator powered linear accelerators to betatrons. The straight lines bounding the points we will call the state-of-the-art curve for X-ray generators.

The spectrum of radiation generated will depend on the target material, beam energy and current. From de Broglie's relationship $E = h\nu$ for the photon energy E in terms of Planck's constant h and the frequency of radiation ν, we conclude that if one electron's energy E_{elec} is converted to only one photon, then it will have a frequency $\nu_{max} = E_{elec}/h$. This corresponds to a wavelength $\lambda_{min} = c/\nu_{max}$ (c = velocity of light). Experimentally the X-ray power output per frequency interval $dI/d\nu$ consists of two parts: the continuous part and spikes due to characteristic radiation. The continuous (Bremsstrahlung portion) is [6, 7]

$$\frac{dI}{d\nu} = \begin{cases} 0 & \text{if } \nu > \nu_{max} \\ i\left[aZ\left(\nu_{max} - \nu\right) + bZ^2\right] & \text{if } \nu \leq \nu_{max} \end{cases} \qquad (2)$$

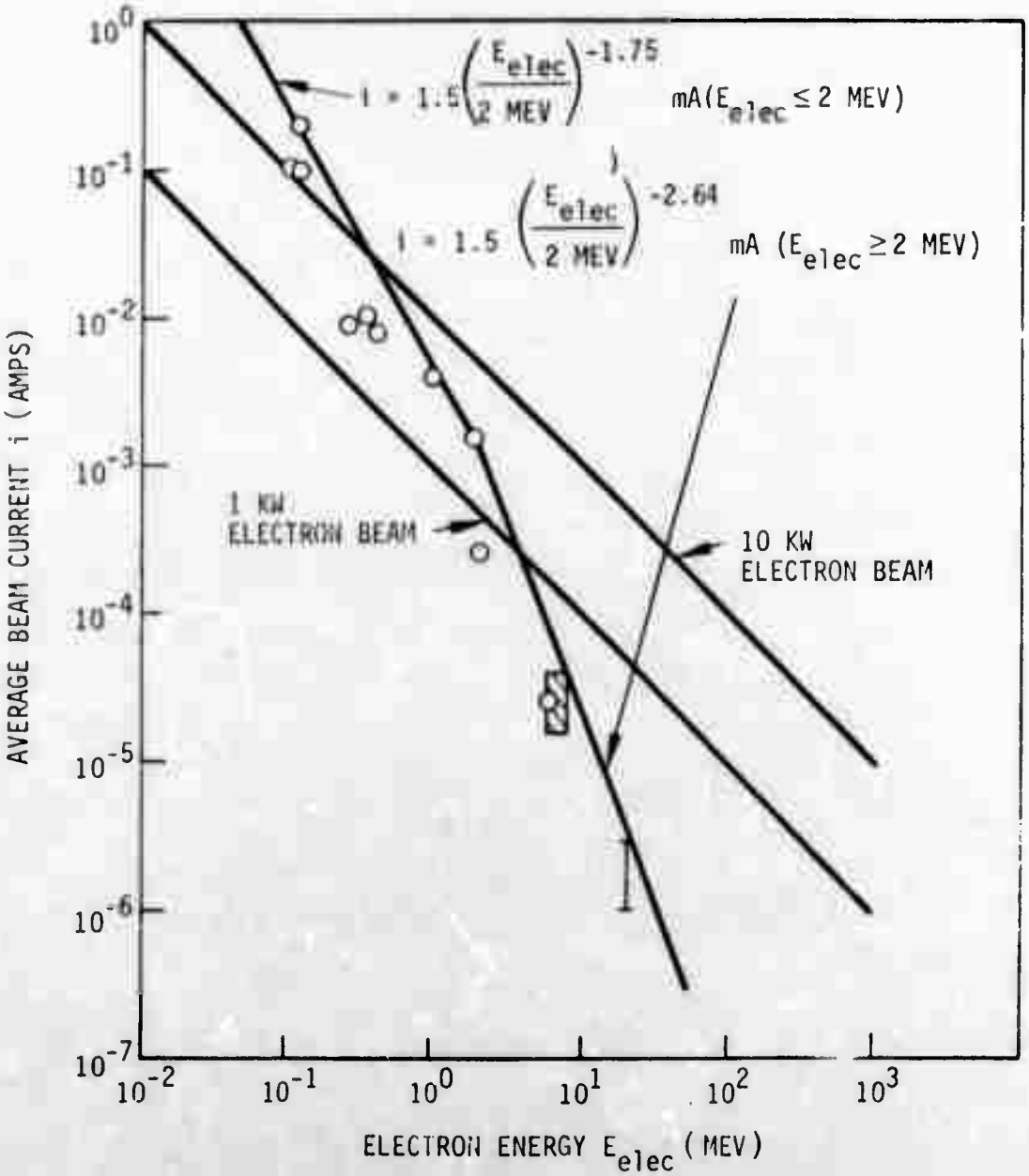

Figure 2-1(U). Typical X-Ray Devices

where i is the electron beam current, Z is the atomic number of the target material, and a and b are constants. For electron energies in the keV region and above, we may take b = 0. Superimposed on this continuous background will be characteristic emission lines of the particular target material, i.e., electrons initially ejected from the target atoms by the incoming electron beam which subsequently have "fallen" back to a ground state with the release of a photon of energy corresponding to the energy of binding (inverse photo-electric effect). With very high energy electron beams, characteristic nuclear γ radiation lines are also observed. In general, these characteristic lines are intense but very narrow, and we will take the emitted X-ray energy spectrum to first order as given by Expression (2) above. Moreover, for simplicity's sake, we will assume Expression (2) is valid even in the relativistic region where very complex analysis is involved. Predicted efficiencies to be obtained later from Expression (2) indicate its gross validity to be within a factor of 2 for a 10 MeV electron beam.

Integration of Expression (2) over all frequencies yields a total power output I of

$$I = \int_0^{\nu_{max}} iaZ \left(\nu_{max} - \nu\right) d\nu = iaZ \frac{\nu_{max}^2}{2} . \qquad (3)$$

The power input is

$$P_{in} = i\Delta V = i \left(\frac{E_{elec}}{e}\right) \qquad (4)$$

where ΔV is the effective potential drop the electrons have fallen through (i.e., 1 keV electron is equivalent to one electron "falling" through a potential drop of 1 kV.) and e is the electron charge. With the use of de Broglie's relation we obtain the efficiency

$$\eta = \frac{I}{P_{in}} = \frac{ea}{2h^2} \; Z \, E_{elec}. \tag{5}$$

Experiments at low energy have determined that $ea/2h^2 \simeq 1.3 \times 10^{-6}$/keV and thus [6, 7]

$$\eta = 1.3 \times 10^{-6} \; z \left(E_{elec}\right) \tag{6}$$

where E_{elec} is in keV.

In terms of efficiency, we express Equation (2) as

$$\frac{dI}{d\nu} = i\eta \left(\frac{2h^2}{eE_{elec}}\right) \left(\nu_{max} - \nu\right).$$

Let dN/dE be the number of photons per energy interval then

$$\frac{dN}{dE} = \frac{1}{h^2 \nu} \frac{dI}{d\nu} = \frac{2P_{in}\eta}{E_{elec}^2} \left(\frac{E_{elec}}{E} - 1\right). \tag{7}$$

Integrating from some arbitrary E_{min} to E_{elec} we obtain the total number of photons N generated with energy greater than E_{min} as

$$N\left(E_{min}, E_{elec}\right) = \frac{2P_{in}\eta}{E_{elec}} \left[ln\left(\frac{E_{elec}}{E_{min}}\right) + \frac{E_{min}}{E_{elec}} - 1\right]. \tag{8}$$

E_{min} will be chosen later so as to optimize the detectability of the objects under investigation. It is this formulation describing the spectra of the number of photons as opposed to intensity spectra which is most convenient for the analysis to follow.

One further effect which will be accounted for is the fact that as the energy of the electron beam is increased, the X-ray production is more

pronounced in the forward direction (parallel to the electron beam). Although relativistic expressions describing this effect exist, we will simply use some experimental values from References 8 and 9 to account for the phenomenon. Table 2-1 shows the half angle $\Delta\theta$ with respect to the forward direction of the beam in which most of the energy of X-rays are emitted.

In Figure 2-2 we show what this concentration of radiation over isotropic radiation is in terms of an effective gain $G(E_{elec})$ as a function of E_{elec}.

As pointed out previously, these formulas are not necessarily valid for relativistic electron beam energies ($E_{elec} \gtrsim 0.51$ MeV). For example, Expression (6) for the efficiency predicts $\eta > 1$ for $Z = 74$ at $E_{elec} \gtrsim 10$ MeV, which is impossible. For this reason, we will alter Expression (6) to

$$\eta = 1 - \exp\left[-1.3 \times 10^{-6} z \left(\frac{E_{elec}}{keV}\right)\right] \qquad (9)$$

which has the correct behavior at low energy and is never greater than one. Figure 2-3 shows the efficiency as a function of E_{elec} for tungsten. In actual fact, the efficiency is a function of target thickness; however, for a first pass analysis, we neglect this, since it is usually less than a factor of two [6, 7].

It should also be noted in passing that there will be the need to dissipate large quantities of heat from the X-ray apparatus. In the low energy limit, due to low efficiency, most of the heat generation will be in the target material. At high energies most of the energy will be dissipated in the X-ray generator shielding. We are assuming only a small hole in the shielding to allow radiation to be shined in the direction of the object to be inspected. The shield will serve to protect associated electronic equipment and also to reduce "space noise" to be discussed

Table 2-1(U). Experimentally Determined Gain of X-Ray Generating Devices Due to Enhanced Forward Bremsstrahlung (U)

BEAM ENERGY E_{elec} (Mev)	HALF ANGLE CONTAINING MOST ENERGY $\Delta\theta$ (DEGREES)	GAIN OVER ISOTROPIC RADIATION $G=2(1-\cos(\Delta\theta))^{-1}$
0.05	90	2.0
0.5	60	4.0
2.0	30	14.9
20.0	4.5	649
100.0	1.5	5840

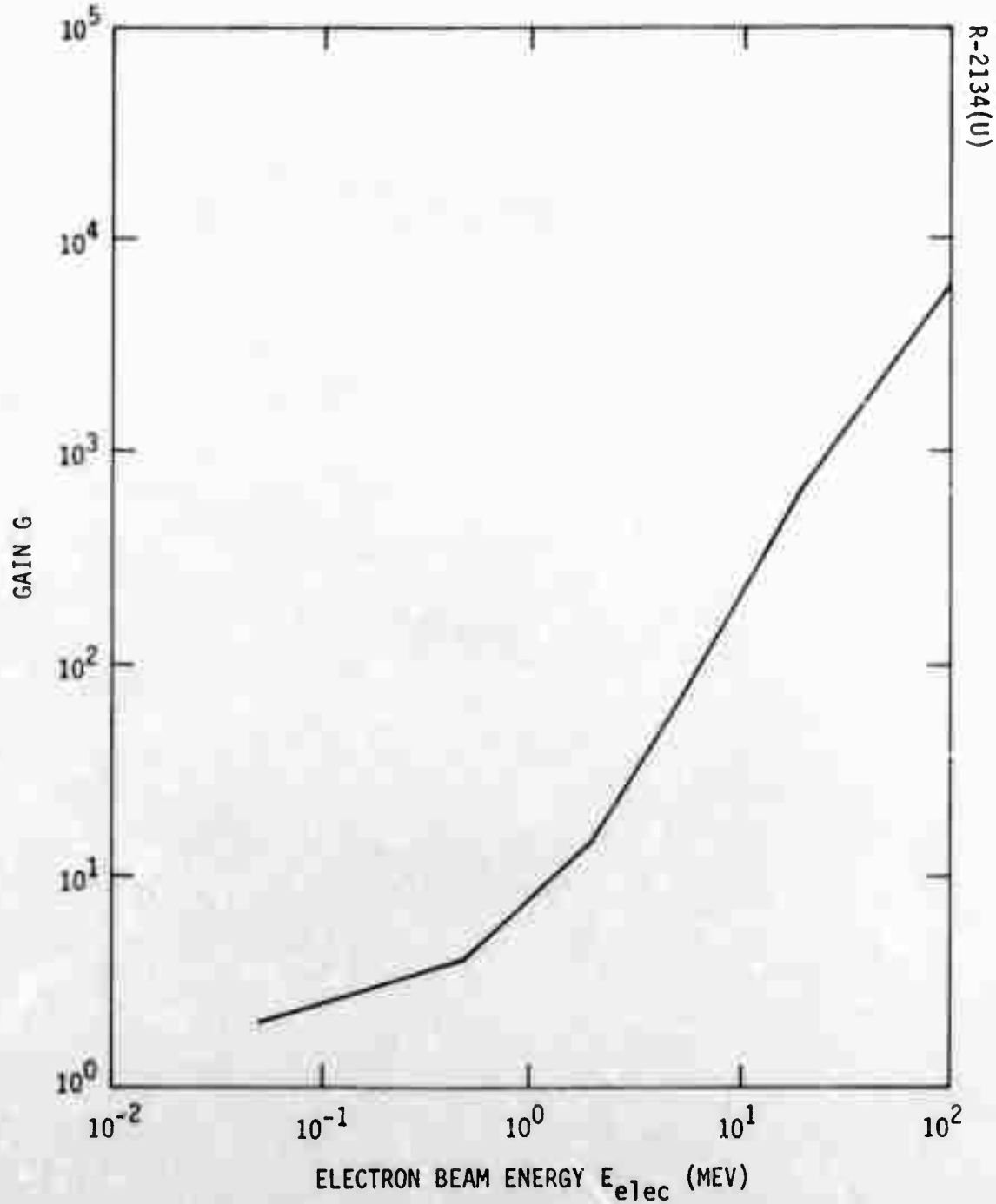

Figure 2-2(U). Directional Gain Over Isotropic Due to Enhanced Forward Bremsstrahlung

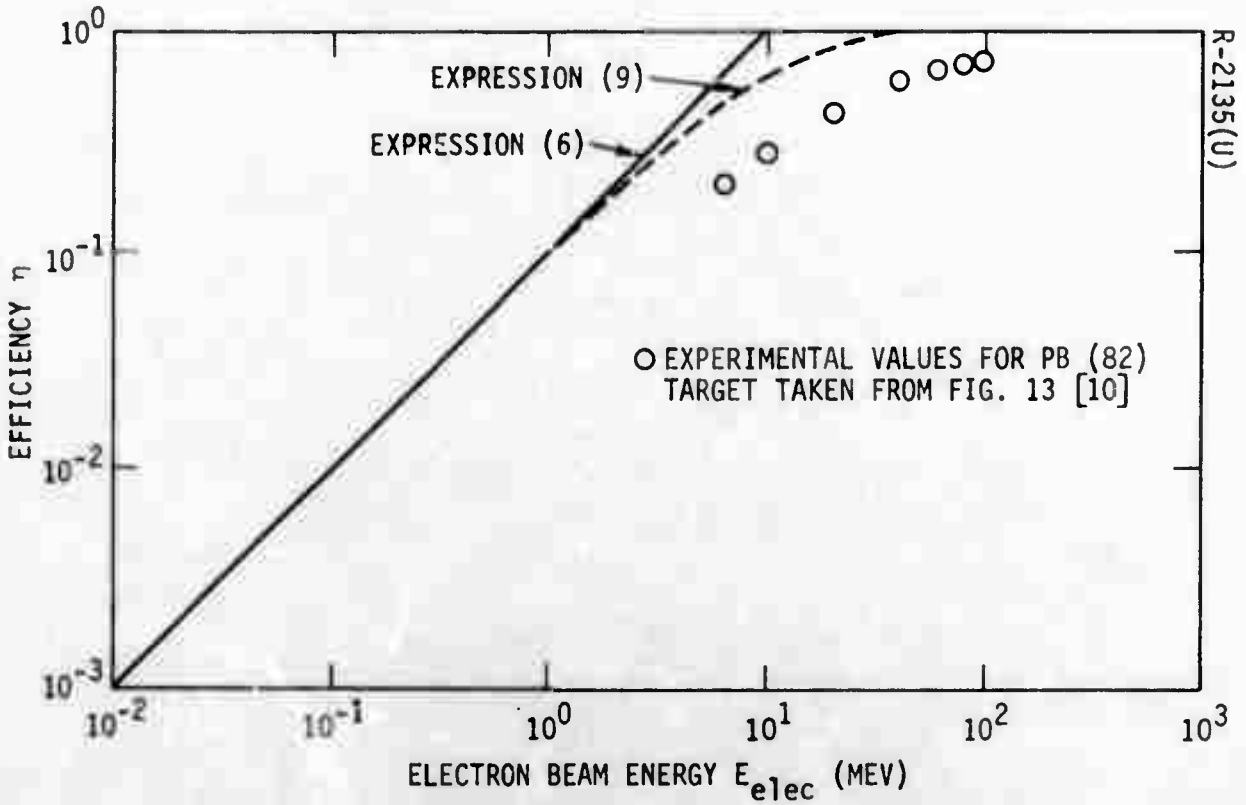

Figure 2-3(U). Efficiency of Conversion of Electron Energy to Radiated Energy for Tungsten Target

later. In general the amount of heat dissipation required will be $\simeq P_{in}$.

In summary then we have a model of an X-ray transmitter in which once the energy of electron beam is specified, the output X-ray spectrum is determined as follows:

Target material fixed at Z = 74

Current $i = i\ (E_{elec})$ from state-of-the-art curve Figure 2-1

Input power $P_{in} = P_{in}\ (E_{elec}) = i(E_{elec})\ \frac{E_{elec}}{e}$

Efficiency $\eta = \eta(E_{elec})$ by Expression (9), Figure 2-3

Gain $G = G(E_{elec})$ Figure 2-2

Number of photons produced per unit time per unit energy $\Big\}$ $\frac{dN}{dE}$ from Expression (7)

Number of photons produced per unit time per unit energy per steradian, radiated in direction of target $\Big\}$ $\frac{d^2N}{dEd\Omega} = \frac{G(E_{elec})}{4\pi}\ \frac{dN}{dE}$ (10)

Figure 2-4 illustrates some typical outputs as a function of electron beam energy for state-of-the-art currents. Note that a factor α increase in state-of-the-art current will raise all data points by a factor α.

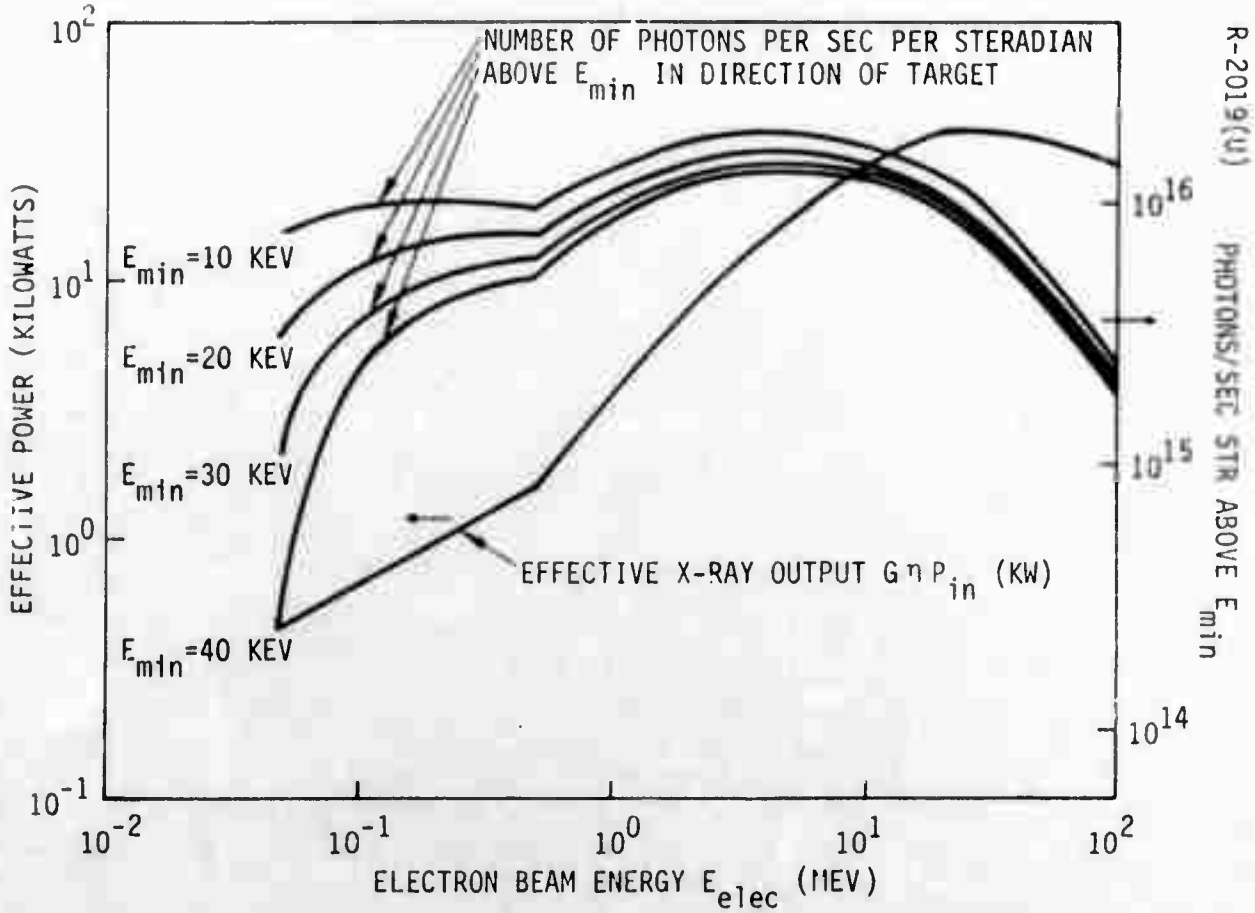

Figure 2-4(U). Bremsstrahlung Output from State-of-the-Art X-Ray Devices

3. THE SPACE ENVIRONMENT

Two aspects of the space environment are of interest. First, what attenuation effects are there on the transmitted and scattered photons; and second, what are sources and intensity spectrums of X-rays in outer space which could influence what the X-ray receiver sees (i.e., background)?

X-rays are absorbed and scattered according to Beer's Law

$$J = J_o e^{-\mu x} \tag{11}$$

where J is the intensity (power) per unit area after traversing a length x of a medium with absorption coefficient μ. This is also valid if J is the number of photons. Based on mass absorption cross sections for air as a function of wavelength [11] and atmospheric density profiles from rocket probes [12], we can construct Table 3-1 of absorption lengths μ^{-1} for which the intensity undergoes one e-fold decrease (i.e., photon mean free path) as a function of height above earth and energy of X-rays.

We notice for 140 km (4.6×10^5 ft) above the surface of the earth that the e-folding distance is 5.48×10^4 km for a 6 keV X-ray. This is the shortest absorption length for heights above this altitude and for energies above 6 keV. Since we will be interested (based on signal to noise considerations) in energies greater than 6 keV and discrimination at heights above 4.6×10^5 ft, we can totally neglect absorption and scattering of X-rays when considering the arrival intensity of the beam.

Note, however, we may have to consider the scattered radiation as a noise source especially if the field of view of the X-ray receiver includes a large volume of X-ray illuminated space containing as many electrons as the scattering target. To estimate this background signal, we can reason as follows:

Table 3-1(U). Typical Absorption Lengths μ^{-1} as a Function of X-Ray Energy and Height Above Earth (U)

HEIGHT (KM)	DENSITY (GM/CM^3)	6 Kev μ^{-1}(KM)	10 Kev μ^{-1}(KM)	20 Kev μ^{-1}(KM)	40 Kev μ^{-1}(KM)	100 Kev μ^{-1}(KM)
60	3.49×10^{-7}	1.19×10^{0}	5.97×10^{0}	3.58×10^{1}	1.15×10^{2}	1.91×10^{2}
100	8.61×10^{-10}	4.84×10^{2}	2.42×10^{3}	1.45×10^{4}	4.65×10^{4}	7.75×10^{4}
140	7.60×10^{-12}	5.48×10^{4}	2.74×10^{5}	1.64×10^{6}	5.26×10^{6}	8.77×10^{6}
180	4.81×10^{-13}	8.66×10^{5}	4.33×10^{6}	2.60×10^{7}	8.32×10^{7}	1.39×10^{8}
220	7.01×10^{-14}	5.94×10^{6}	2.97×10^{7}	1.78×10^{8}	5.71×10^{8}	9.51×10^{8}

Since the absorption length is so large at altitudes of interest, we can consider only the single scattering events as predominating. Consider a volume element dV of space. Let $d\sigma_c(E,\theta)/d\Omega$ be the differential Compton cross section of an electron for a photon of energy E, with θ the angle subtended at the given point in space under consideration by the X-ray transmitter and X-ray receiver. Furthermore, let ρ_e be the number density of both bound and free electrons, then the number of photons per unit time scattered per steradian per unit volume is,

$$\frac{d^3N}{dVd\Omega dE} = J\rho_e \frac{d\sigma_c(E,\theta)}{d\Omega} \tag{12}$$

where J is the incident number flux of photons per unit area per unit time per unit energy. The scattered spectrum will be shifted in energy according to the appropriate Compton energy shift which is a function of θ and E. We will refer to this background as "space noise". To obtain the total received photons, we must integrate over the appropriate volume of space which will depend on the particular geometry. In general, this background will decrease with a decrease in receiver field of view.

There are other extraterrestrial sources of X-rays, namely the sun, certain galaxies and X-rays coming up from the earth caused by solar wind and cosmic ray interaction with the upper atmosphere. These X-ray fluxes have been measured by instrumentation on space probes and high altitude balloons. The investigation of these sources has given birth to a new field of science called X-ray astronomy and it is from the developing technology in this area that a large amount of this report is based.

A number of X-ray sources in the universe have been discovered in the last decade mainly by means of X-ray detectors aboard satellites or rocket probes. Among galactic sources are the Crab Nebula and Sco X-1 whose flux spectrums are shown in Figures 3-1 and 3-2. One moderately strong extra galactic source M-87 (Figure 3-3) has also been observed. Many

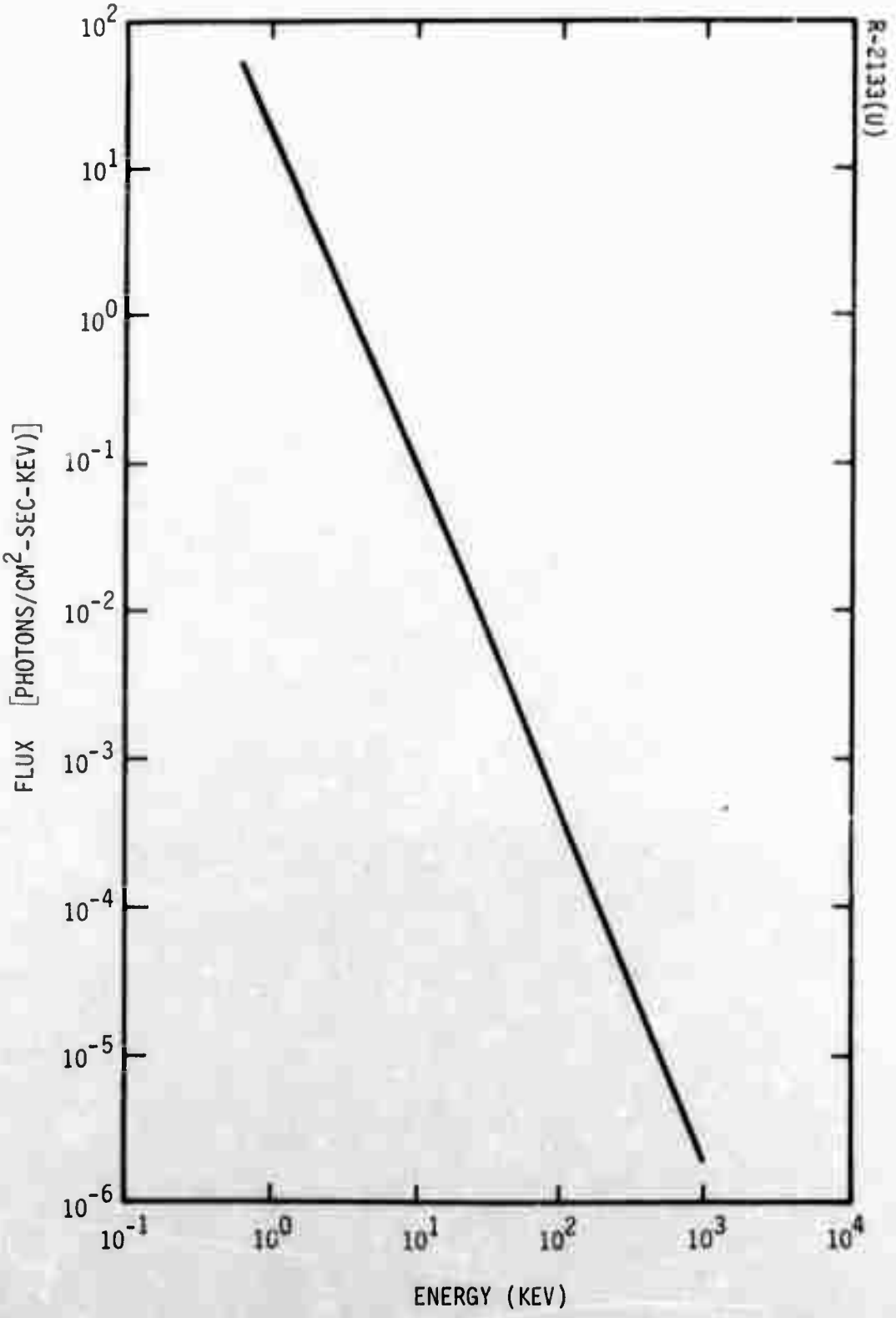

Figure 3-1(U). X-Ray Flux Spectrum from Crab Nebula [13]

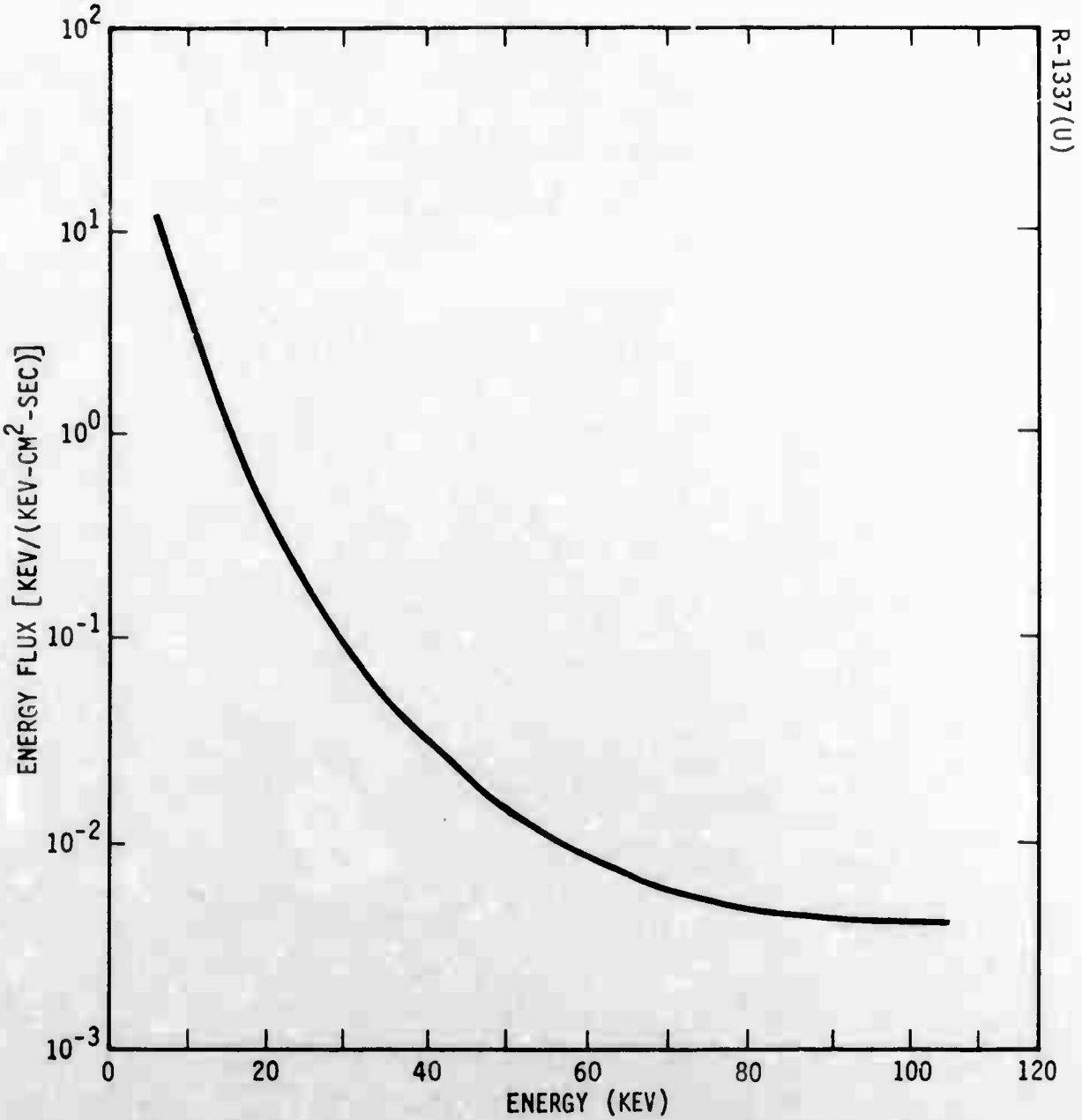

Figure 3-2(U). X-Ray Energy Flux Spectrum from SCO X-1 [14]

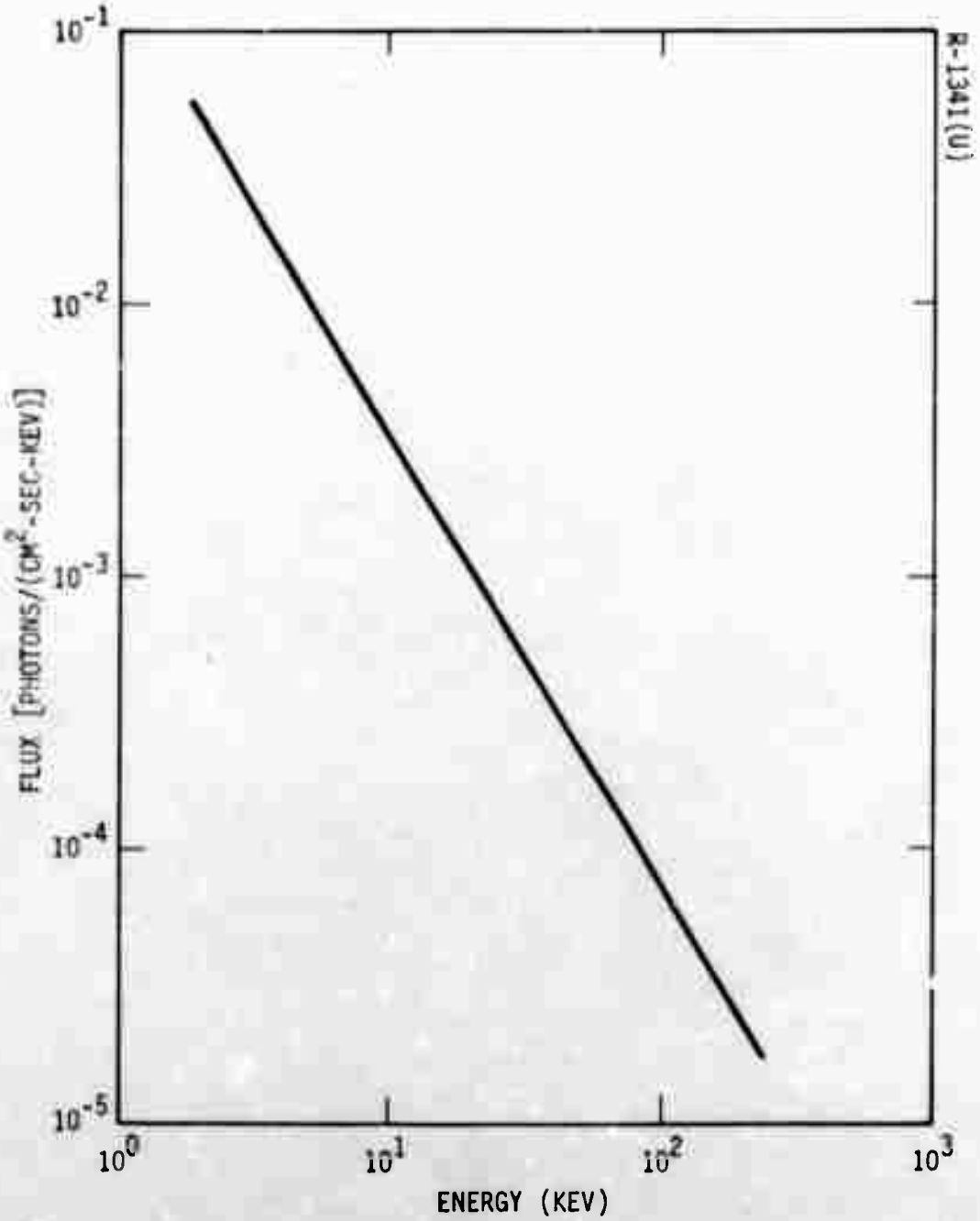

Figure 3-3(U). X-Ray Flux Spectrum from M-87 [15]

other sources have been reported; however, "false alarm" rates may be large. Moreover, our own sun's corona is a source of X-rays equivalent to a grey body emission of a few million degrees Kelvin, see Figure 3-4. In general, however, solar radiation falls off exponentially as energy increases and the solar X-rays flux become less than other X-ray sources at large energy. For example, Crab Nebula has greater flux than the sun for energies above about 10 keV.

These X-ray sources need only be worried about if they are in the field of view of the X-ray detector. The angular size of these objects is very small (Sun ≈ 30 feet; Crab ≈ 3 feet) and our receiver angular resolution will also be small so we will, therefore, assume for simplicity's sake that we do not have them in the X-ray receiver field of view.

Besides these striking X-ray features, there is a diffuse X-ray background probably due to a large number of low level X-ray emitters of galactic origin. We will assume this flux is isotropic as was once thought to be the case. In actual fact, it varies slightly for viewing galactic equator versus galactic pole [17]. Figure 3-5 shows the photon spectrum of this diffuse (isotropic) X-ray background. It should be noted that almost all data on diffuse background above ∿10 kcV are obtained with sensors having a field of view angle of a few to many degrees; thus, there is the possibility that if our receiver has much finer resolution than this, the diffuse nature of this background radiation may disappear.

The earth is also a source of X-rays, if one views it from space, due to a number of very complex interaction processes including:

a) cosmic rays impinging on the earth's atmosphere (flux ∿1/cm^2 sec, mostly protons of average energy ∿3 BeV) cause generation of X-rays through cascade-like phenomena;
b) some fraction of X-rays impinging on the earth's atmosphere are scattered back into space, i.e., earth albedo X-rays.

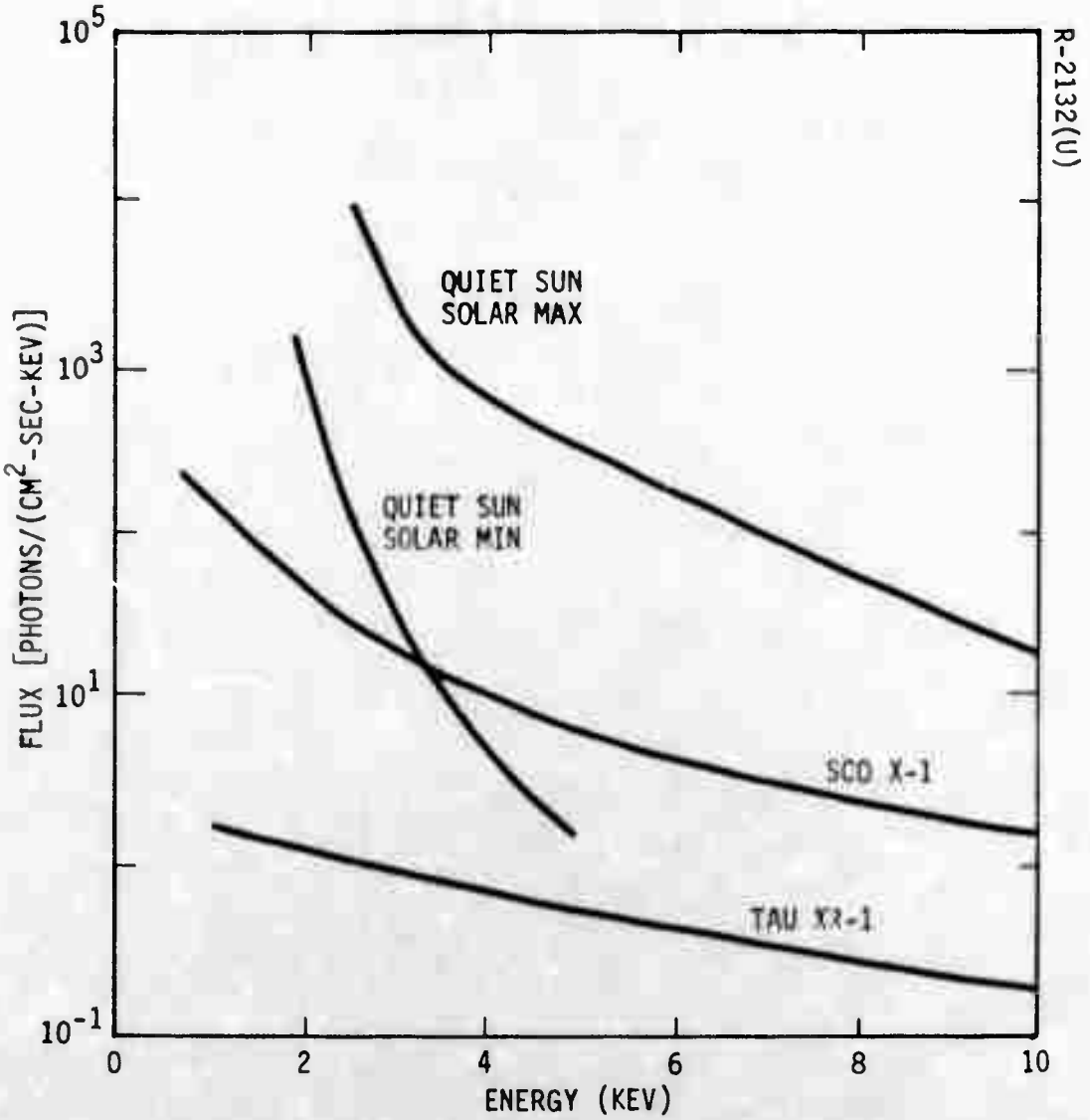

Figure 3-4(U). Solar Flux Spectrum Compared to Other Discrete Sources [16]

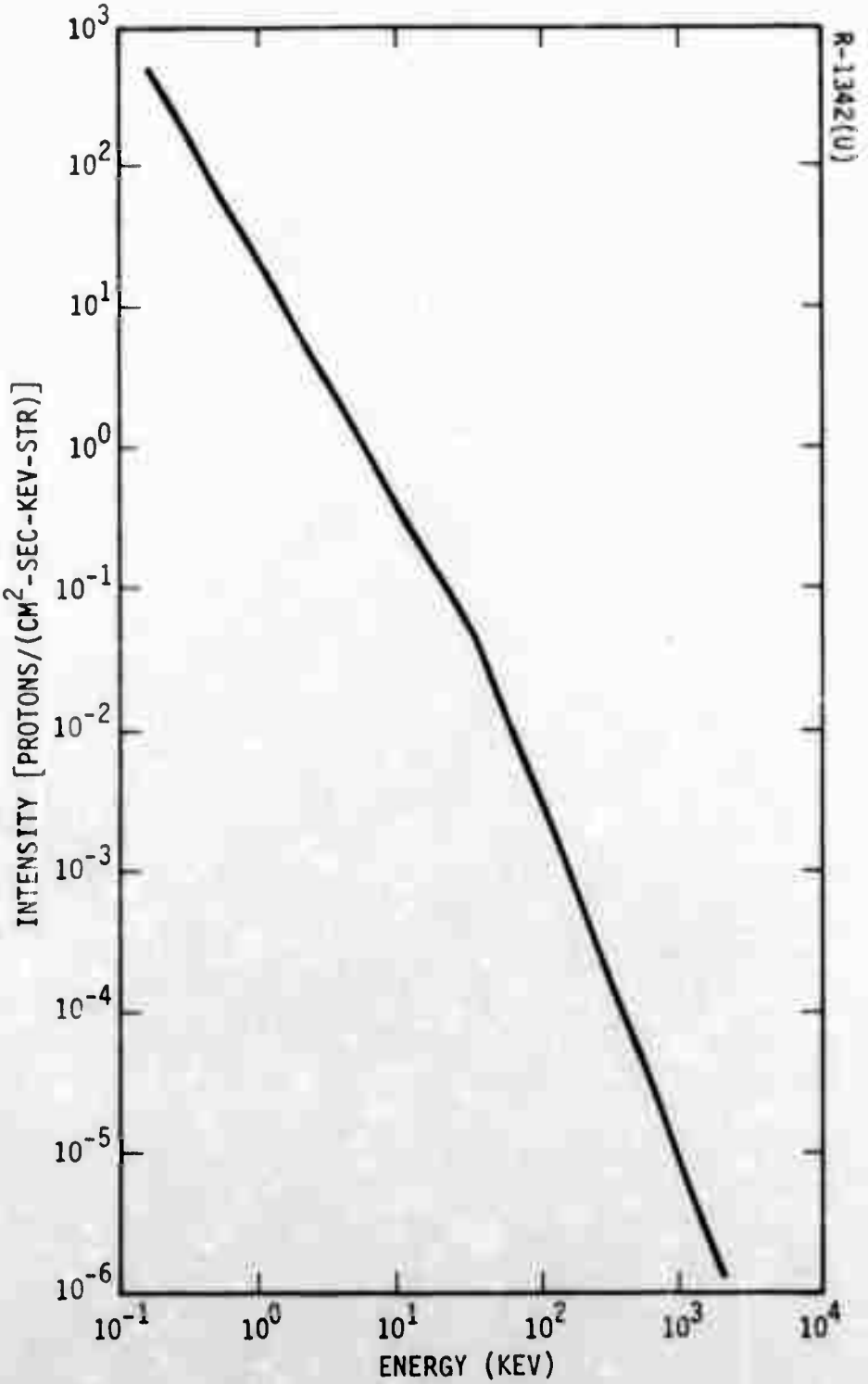

Figure 3-5(U). Diffuse X-Ray Background Spectrum [13]

For balloon measurement corrections (looking up), Peterson [13] has published a density independent source function $S_o(E)$ for X-ray production per (gm · sec · keV) due to cosmic rays, see Figure 3-6. In actual fact, it probably includes more than just cosmic ray effects. Assuming this result is valid looking down from space, we can reason as follows: Let dN_{Earth}/dE be the number of photons coming up from the earth (looking normal to earth's atmosphere) per (keV · steradian · cm^2 · sec), then

$$\frac{dN_{earth}}{dE} = \frac{S_o(E)}{4\pi} \int_o^{r_{max}} \exp\left(-r/\lambda(E)\right) dr = \frac{S_o(E)\lambda(E)}{4\pi}\left[1 - \exp\left(-\frac{r_{max}}{\lambda(E)}\right)\right]. \quad (13)$$

In this expression $\lambda(E)$ is the mean free path for photons of energy E in the earth's atmosphere in gm / cm^2 units (i.e., inverse mass absorption coefficient), and r_{max} is the maximum thickness of atmosphere in gm/cm^2 units $\sim 10^3$ gm / cm^2. For all energies of interest, the exponential term is negligible. Using $\lambda(E)$ from Reference 11 we obtain the results in Figure 3-7. These are in slight disagreement with results measured by Brini et. al. [18] shown in Figure 3-8.

We note that the earth X-ray spectrum is less than the diffuse X-ray background at low energies but may be on the same order for energies of a few hundred keV. Note that Figure 3-7 is for looking straight down only and probably is dependent slightly on angle with respect to normal. In fact high energy (many MeV) measurements indicate the earth is a stronger flux source than space and there is a higher flux from the earth's limb than for normal incidence [17].

In conclusion, the space environment causes negligible attenuation of the transmitted and received X-ray beams. But, it does impose background levels of X-rays which will tend to conceal the scattered X-ray signals from the targets. The background sources of most concerns are "space noise", "earth shine", and diffuse cosmic background. Space noise is

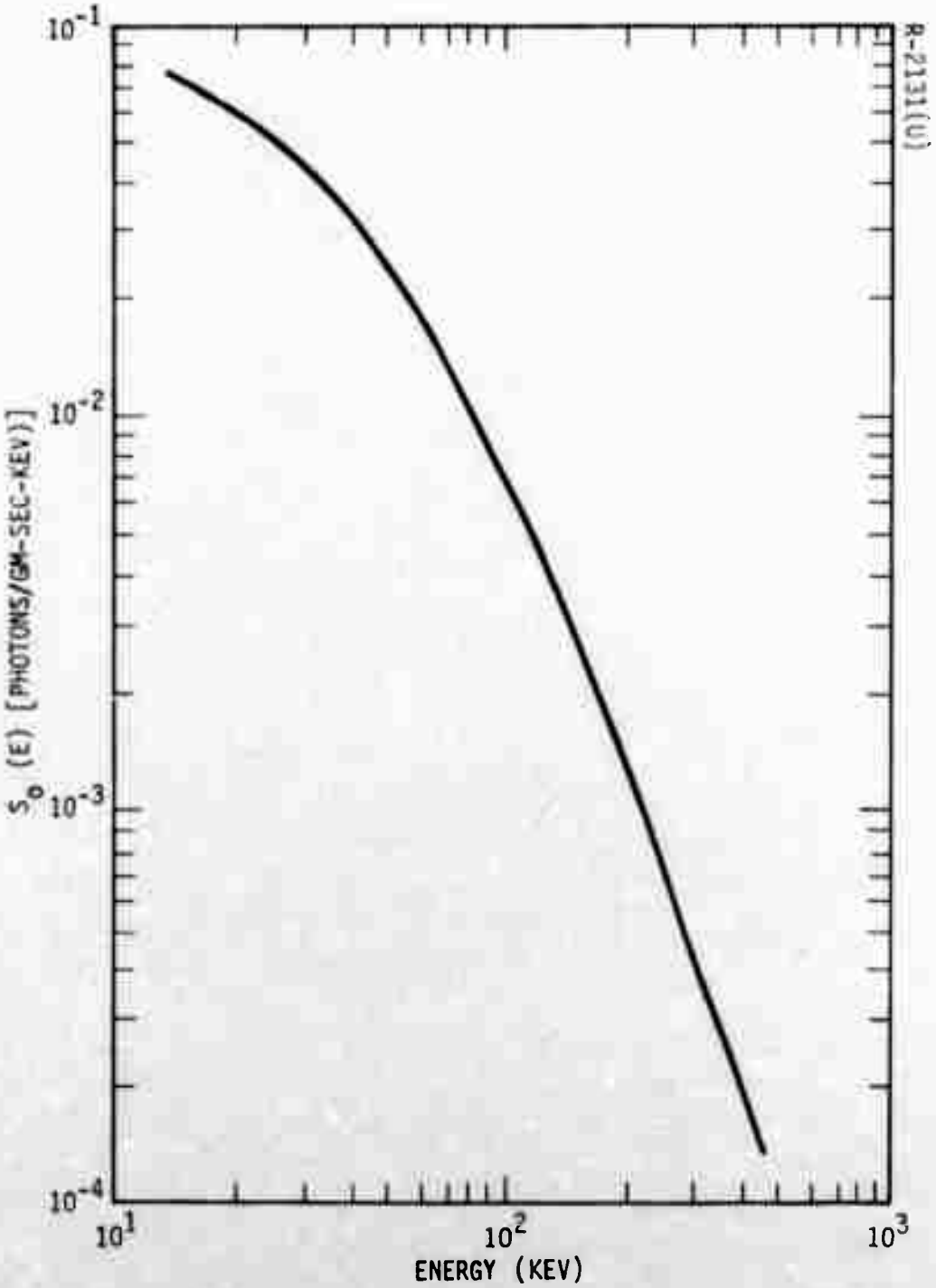

Figure 3-6(U). Source Function for the Production of X-Rays by Cosmic Ray Interaction with Atmosphere [13]

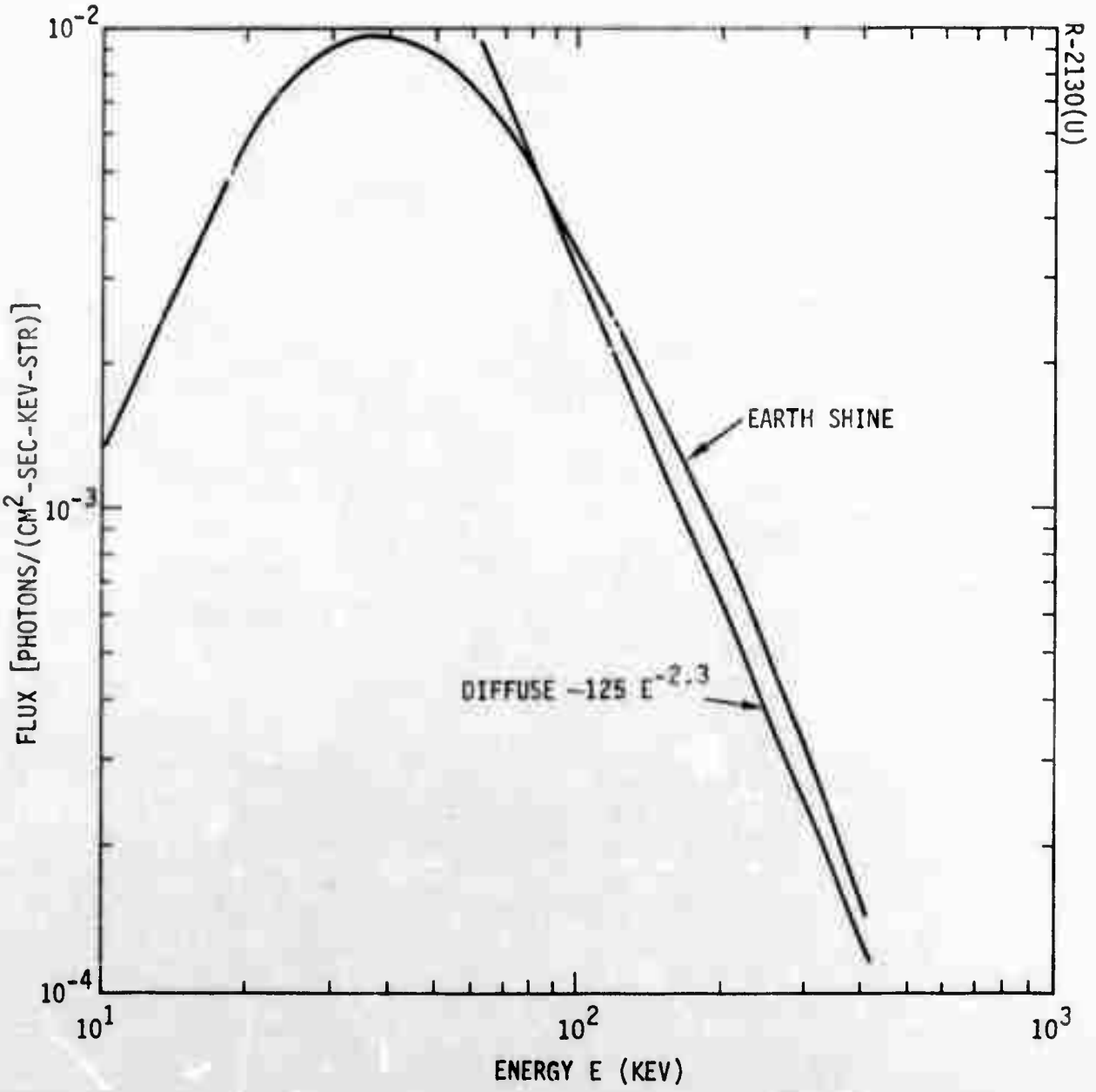

Figure 3-7(U). Calculated "Earth Shine" Flux Spectrum

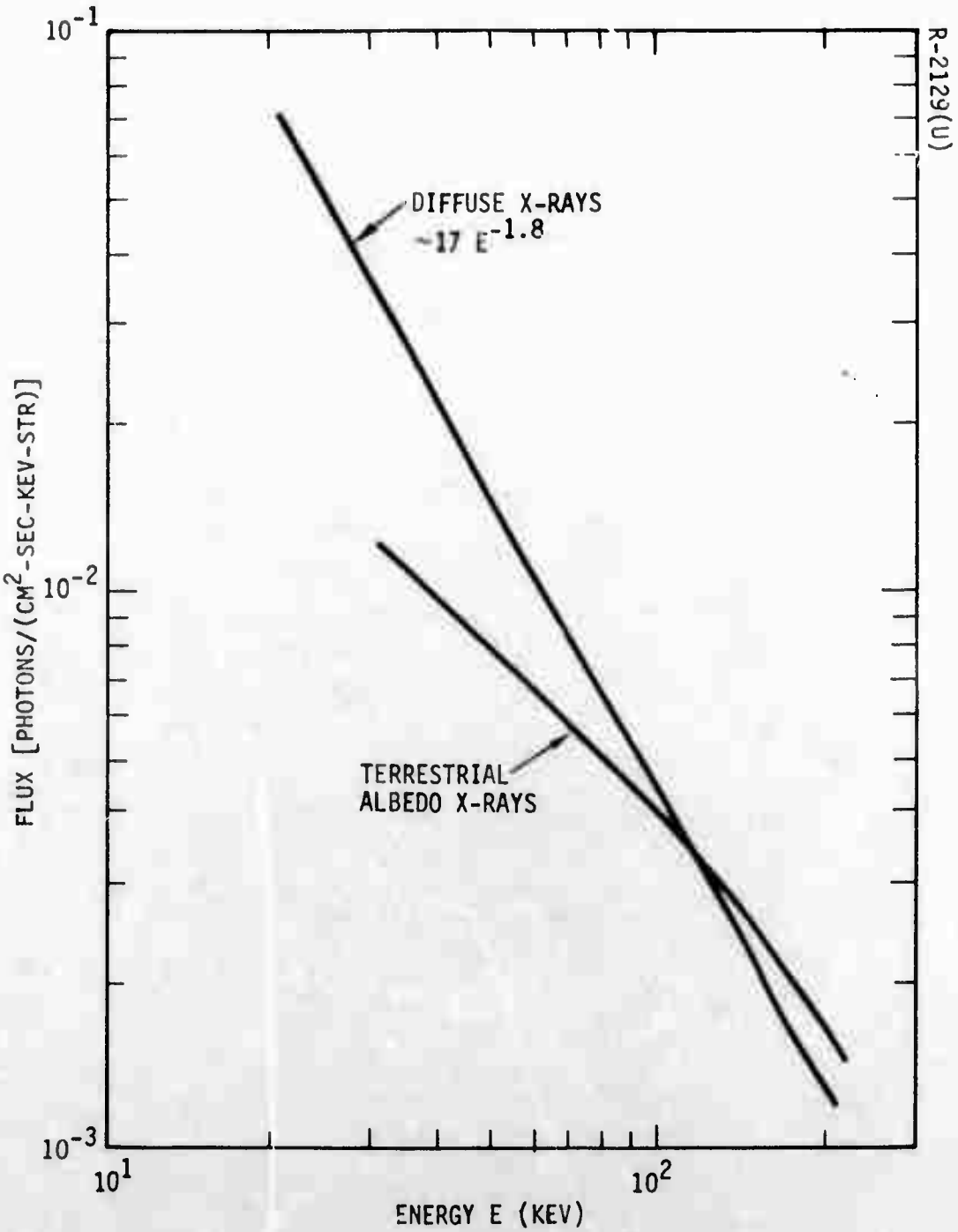

Figure 3-8(U). Measured "Earth Shine" X-Ray Flux Spectrum [18]

obtained from Expression (12), earth shine will have a spectrum similar to Figure 3-7, and for the diffuse component (Figure 3-5) we will assume the fit

$$\left(\frac{dN}{dE}\right)_{\text{diffuse}} = \left\{ \begin{array}{l} 16.2\ (E/\text{keV})^{-1.7} \text{ if } E \leq 30 \text{ keV} \\ 125\ (E/\text{keV})^{-2.3} \text{ if } E \geq 30 \text{ keV} \end{array} \right\} \text{Photon/keV sec cm}^2 \text{ steradian.} \qquad (14)$$

4. THE TARGETS AND THEIR SCATTERING

For the physical characteristics of the reentry vehicles (RV) and replica decoys (RD), we have taken some typical parameters from a recent MCD threat study [1]. These characteristics are listed in Table 4-1.

The scattering and absorption of X-rays by the RV and RD is a very complicated process involving photoelectric absorption, Auger effect, fluorescence, Compton scattering and for photons with energy greater than 1.1 MeV pair production. The geometry is such that the incoming beam width is greater than the physical size of the object. The only practical means to obtain an accurate estimate of the scattering for such a complicated geometry would be a three-dimensional Monte Carlo computer algorithm. While such codes do exist [19], they are too cumbersome for exploratory calculations.

For order of magnitude arguments, it would probably be sufficient to assume that all radiation impinging on the target is scattered isotropically. However, with little added effort, a better approximation for the back scattering case can be made.

For the case of backscattering, we can approximate the RV and RD as flat slabs of homogeneous composition consistent with their true chemical make-up and of thicknesses twice their skin thicknesses. We have neglected the internal components of the RV for simplicity sake. For single back scattered events, the energy of the photon will not exceed $\sim$0.51 MeV, and thus if the back scattering occurs deep inside the weapon, it probably won't make its way out. Assuming that the only interaction processes are photoelectric absorption and Compton scattering, we can estimate the amount of radiation "reflected" (or albedo) in the following matter. If μ_t is the total attenuation coefficient and

$$\mu_t = \mu_a + \mu_s \tag{15}$$

Table 4-1 (U). Typical Threat Parameters (U)

RV: WEIGHT ~ 5000 LBS
SKIN COMPOSITION:
0.75 IN. ABLATIVE SHIELD (DENSITY 1.35 GM/CM^3)
40% PHENOLIC RESIN
60% ASBESTOS (DENSITY 2.77 GM/CM^3)
0.13 IN. ALUMINUM SUBSTRUCTURE (DENSITY 2.77 GM/CM^3)

RD: WEIGHT ~ 50 LBS
SKIN COMPOSITION:
0.045 IN. CARBON CLOTH (DENSITY = 0.238 GM/CM^3)
0.017 IN. BUTYL/NOMEX SEALANT (DENSITY = 1.06 GM/CM^3)

RV AND RD:
SHAPE - APPROXIMATELY A FRUSTUM OF HEIGHT 10 FT, BASE RADIUS 3.33 FT AND TOP RADIUS 1 FT
VOLUME - 162 FT^3
AREA - 174 FT^2
PRESENTED AREA - SIDE 43 FT^2
- BASE 35 FT^2

DEPLOYMENT CHARACTERISTICS:
DEPLOYED ~ 350 SECS AFTER LIFT OFF
APOGEE ~ 1000 SECS AFTER LIFT OFF
MAXIMUM VELOCITY IMPARTED TO RV OR RD
CROSS TRAJECTORY ~ 75 FT/SEC
ALONG TRAJECTORY ~ 300 FT/SEC
APPROXIMATE VELOCITY OF RV OR RD ~ 22,000 FT/SEC
DEPLOYMENT HEIGHT ~ 0.6 to 1.2 x 10^6 FT DEPENDING ON γ OF REENTRY
APOGEE HEIGHT ~ 2 to 5 x 10^6 FT DEPENDING ON γ

where μ_a is the photoelectric absorption coefficient and μ_s is the scattering coefficient then the ratio of scattered I_s to incident I_o (number) intensity after passing through a thickness x is

$$\frac{I_s}{I_o} = \frac{\mu_s}{\mu_t}\left(1 - e^{-\mu_t x}\right). \tag{16}$$

We will simply use the differential form of this in terms of the $d\Omega$ steradian into which the scattering occurs, i.e.,

$$\frac{1}{I_o}\left(\frac{dI_s}{d\Omega}\right) = \left(\frac{d\mu_s}{d\Omega}\right)\frac{\left[1 - \exp\left(-\mu_t x\right)\right]}{\mu_s + \mu_a}. \tag{17}$$

Assuming that the Klein-Nishina Compton scattering formula [20] for free electrons describes the scattering, we obtain

$$\frac{1}{I_o}\left(\frac{dI_s}{d\Omega}\right) = \frac{\frac{N_A Z}{A}\left(\frac{d\sigma_c(\theta,E)}{d\Omega}\right)}{\frac{\sigma_c(E) N_A Z}{A} + \frac{\mu_a}{\rho}}\left(1 - \exp\left(-\mu_t x\right)\right) \tag{18}$$

where Z/A is the ratio of atomic number to atomic weight of the material, N_A is Avogadro's number, ρ is the mass density, $d\sigma_c(\theta, E)/d\Omega$ is the differential Compton cross section and

$$\sigma_c(E) = 4\pi\int\left(\frac{d\sigma_c(\theta, E)}{d\Omega}\right)d\Omega.$$

We now assume that all scattered radiation is not further attenuated and we integrate over the backward 2π steradians. The result can be cast in the form

$$\text{Albedo} = \frac{I_s}{I_o} = \frac{\frac{3}{8}\int_{-1}^{0}\frac{(1+\bar{x}^2)\left[1 + \frac{\gamma^2(1-\bar{x})^2}{(1+\bar{x})(1+\gamma[1-\bar{x}])}\right]}{\left[1 + \gamma\left(1 - \bar{x}\right)\right]^{\beta}}d\bar{x}}{\frac{\sigma_c(E)}{\sigma_o} + \frac{\mu_a}{\rho}\left(\frac{A}{\sigma_o N_A Z}\right)}\left(1 - e^{-\mu_t x}\right) \tag{19}$$

where $\sigma_0 = 0.666 \times 10^{-24}$ cm^2 is the classical Thomson cross section, γ is the energy of the impinging X-rays in units of the rest mass of an electron and the exponent β is 2 for number albedo and 3 for energy albedo.

Based on the description in Table 4-1, we have constructed approximate mass absorption coefficients as a function of wavelength for the various constituents of the RV and RD in Table 4-2. The first seven materials listed are taken from Reference 5 and are the basic mass absorption coefficients upon which the latter entries are based using the usual relative mass weighting of the individual constituents [7]. Evaluation of Expression (19) using results in Table 4-2 are shown in Figure 4-1 for the RV and RD. Mass absorption coefficients at wavelength not given in the table are obtained by a linear log-log interpolation.

Using the same procedure for semi-infinite slabs yield good agreement in energy albedo for hydrogen given by Raso et. al. [21] in the range from 20 keV to 1 MeV. The same calculation for iron is a factor 3 above Raso's results but has the correct shape. Considering the unusually naive assumptions inherent in Expression (19) this is surprising. We conclude that the predicted albedos in Figure 4-1 may be a factor of 2 high, however, we expect the general shape to be correct. The decrease in albedo at low energy is due to dominance of photoelectric effect over scattering and the falloff in number albedo at large energies is due to de-enhanced Compton backscattering at high energy. The energy albedo falls off for the same reason plus loss of energy per photon due to Compton shift in energy. Note that we have not accounted for the effect of the weapon material (lots of high Z) in the RV albedo. It seems reasonable it would decrease the albedo by about one fourth, which is about the amount of the back skin shielded by the weapon, i.e., (weapon area $\sim$ 1/2 presented area).

In terms of the quantity S in Expression (1), the most naive assumption would be isotropic scattering of all incident radiation ($S = 1/4\pi$), and we feel a better (although still in error) approximation is

Table 4-2 (U). Mass Absorption Coefficients (μ/p) in CM^2/GM as a Function of Wavelength for the Various Materials of Interest (U)

WAVELENGTH (A^o) / MATERIAL (A/Z)	0.01	0.05	0.10	0.50	1.00	5.00
H (1.01)	0.1134	0.2252	0.2794	0.3660	0.3939	1.984
C (2.00)	0.0571	0.1135	0.1419	0.3357	1.402	144.3
N (2.00)	0.0571	0.1136	0.1428	0.4376	2.208	236.4
O (2.00)	0.0571	0.1138	0.1440	0.5769	3.305	356.5
Mg (2.03)	0.0563	0.1134	0.1505	1.594	11.21	1097.
Al (2.08)	0.0551	0.1112	0.1502	1.950	13.95	1304.
Si (2.01)	0.0570	0.1155	0.1588	2.420	17.51	1591.
ASBESTOS (1.98)	0.0574	0.1152	0.1507	1.304	8.915	859.0
PHENOLIC RESIN (1.86)	0.0616	0.1215	0.1537	0.4274	2.026	211.4
ABLATOR (1.93)	0.0591	0.1177	0.1519	0.9533	6.159	600.0
BUTYLE RUBBER (1.75)	0.0650	0.1291	0.1611	0.3399	1.261	124.4
NYLON (1.83)	0.0627	0.1246	0.1560	0.3847	1.6[illegible]4	170.8
BUTYL - NOMEX SEALANT (1.79)	0.0639	0.1268	0.1586	0.3623	1.463	147.6
R.V. (1.97)	0.0580	0.1160	0.1515	1.212	8.185	783.0
R.D.#1 (1.89)	0.0605	0.1202	0.1503	0.3490	1.432	145.9

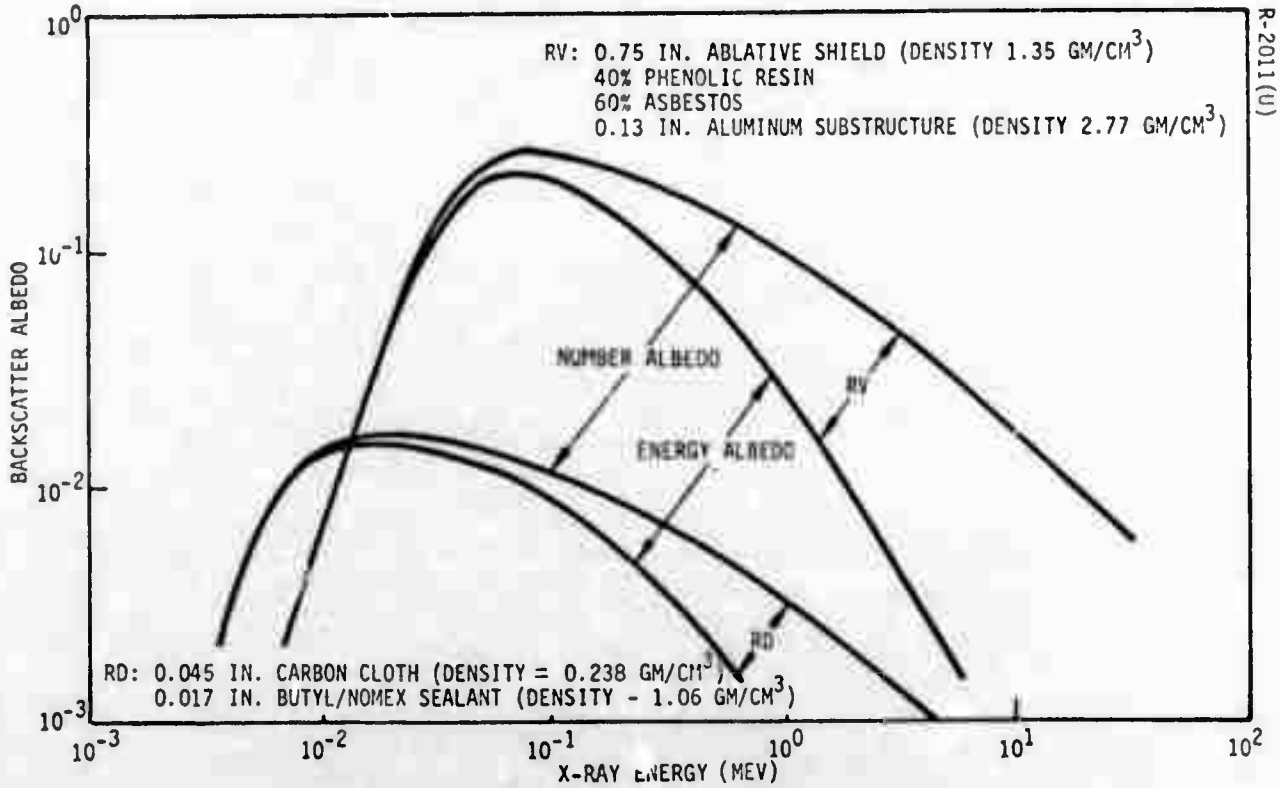

Figure 4-1(U). RV and RD Skin Albedos

$$S = \frac{1}{2\pi} \text{ (albedo)} \tag{20}$$

where albedo is number albedo if interested in number (of photons) flux and energy albedo if concerned with energy flux.

If we denote by θ the angle subtended at the target by the transmitter and receiver, then in general the ratio S of scattered radiation per steradian in direction of receiver to incident radiation is a function of θ as well as energy E of incident radiation, i.e.,

$$S = S(\theta, E). \tag{21}$$

Expression (20) is our approximation for S when $\theta = 0$. The arbitrary θ case is far too complex for a simple analysis. In general, S will increase in the $\theta \to 180°$ direction at high energies due to enhanced forward Compton scattering. Folding in of the absorption process will be very geometry dependent at intermediate and low energies. Therefore, we will use only the rough approximate Expression (20) for backscattering.

The steradian of the incident beam of X-rays which the target intercepts is A_T/R_T^2 and the target is thus illuminated by a spectrum

$$\left(\frac{dN}{dE}\right)_{\text{on target}} = \left(\frac{A_T}{R_T^2}\right) \frac{d^2N}{dE d\Omega} . \tag{22}$$

On the average only $S(\theta, E)$ of the incident photons in energy interval near E will be scattered per steradian in the direction of the receiver, where θ is the angle subtended at the target by the receiver and transmitter. Due to the Compton scattering process, there will be a shift in the wavelength [7]

$$\Delta\lambda = \lambda_{\text{scat}} - \lambda_{\text{in}} = \lambda_c(1 + \cos\theta) \tag{23}$$

where λ_c is 0.0243 A° ($=h/m_e c$), λ_{scat} is the scattered radiation wavelength and λ_{in} is the incident wavelength. This corresponds to an energy shift

$$E_{scat} = E_{in} \Big/ \left[1 + \frac{E_{in}}{E_c} (1 + \cos\theta)\right] \tag{24}$$

or

$$E_{in} = E_{scat} \Big/ \left[1 - \frac{E_{scat}}{E_c} (1 + \cos\theta)\right] \tag{25}$$

where E_{scat}, E_{in} and E_c are hc/λ_{scat}, hc/λ_{in} and hc/λ_c respectively.

The resulting spectrum from this target in the direction of the receiver per steradian is then

$$\left(\frac{d^2N}{dE_{scat}\,d\Omega}\right)_{\substack{\text{toward}\\ \text{receiver}}} = S(\theta, E_{in}) \left(\frac{dN}{dE_{in}}\right)_{\text{on target}} \frac{dE_{in}}{dE_{scat}} . \tag{26}$$

Differentiating Equation (25) yields

$$\frac{dE_{in}}{dE_{scat}} = \left[1 - \frac{E_{scat}}{E_{in}} (1 + \cos\theta)\right]^{-2} = \left(\frac{E_{in}}{E_{scat}}\right)^2 \tag{27}$$

which helps to case Expression (26) into the form

$$\left(\frac{d^2N}{dE_{scat}\,d\Omega}\right)_{\substack{\text{toward}\\ \text{receiver}}} = \left[S(\theta, E_{in}) \left(\frac{dN}{dE_{in}}\right)_{\substack{\text{on}\\ \text{target}}} \left(\frac{E_{in}}{E_{scat}}\right)^2\right] \tag{28}$$

$$E_{in} = \frac{E_{scat}}{\left[1 - \frac{E_{scat}}{E_c} (1+\cos\theta)\right]} .$$

Expression (28) defines the spectrum scattered in the direction of the receiver, and will constitute the signal to be "looked for" by the receiver.

5. THE X-RAY RECEIVER

The function of the receiver is to pick up the scattered X-ray signal from the RV or RD with sufficient steradian resolution to be of use to some other sensor which will take over tracking after the discrimination function is performed. Note that we use the terms X-ray and γ-ray loosely and interchangeably.

X-ray astronomers have experimented with a number of so-called "X-ray telescopes" [22,23]. In practice, grazing incidence reflection in conjunction with photographic film are used below 1 keV, gas proportional counters are used in the 1 - 20 keV energy range, scintillation counters in the 20 keV → 1 MeV region, and in the high energy region devices employed are combinations of scintillation, spark chamber, and Cherenkov radiation detectors.

Grazing incidence optics relies on the property that the index of refraction of X-rays is less than one with the result that total reflection at small angles is possible for X-ray impinging on polished materials. As the energy increases, the angles necessary decrease and resulting collection efficiency is decreased.

The proportional counters have been extensively used mainly because they can be built with very large effective collecting area. In conjunction with a modulation collimator, they have given the most accurate position measurements of extra-terrestrial X-ray sources. At higher energies the amount of gas is not sufficient to cause X-rays to interact and, therefore, efficiency decreases.

For the scintillation counters, coincidence and anti-coincidence techniques are used to define directionality of counted X-ray events. When energy of X-rays are in the few hundred keV and higher region, all matter becomes transparent and efficiency decreases.

In the very high energy γ-ray ranges, it is the detection of pair-production components, positrons and electrons, which is used to detect the presence of photons.

Since the peak albedos in Figure 4-1 are within the working range of scintillation counters mentioned above, this is probably the type of detector necessary for the X-ray discrimination system. The most often used general configuration consists of four scintillation crystals, pictured in Figure 5-1, obtainable from Harshaw Chemical Corporation on special order. The frontal cylindrical CsI crystal with holes drilled defines a resolution half angle θ_{res}. Directly behind this is a thin cylinder of NaI(Tl) of smaller radius than the frontal crystal, and behind this is another CsI crystal of the same radius but of thickness comparable to the frontal crystal. These latter two crystals in combination are termed a "phoswitch" and are viewed by one large photomultiplier tube from the rear. Surrounding this phoswitch is an annulus crystal of NaI(Tl) viewed by six photomultiplier tubes. The frontal crystal is viewed by four photomultipliers. The entire arrangement is housed typically in an aluminum chassis, and there is typically a beryllium or aluminum "window" in front of the holes of the frontal crystal. The frontal and annulus crystals and the phoswitch are optically decoupled by aluminum foil to prevent scintillation radiation (typically $\sim$ 3000 → 5000 Å) from traversing more than one component crystal.

When X-rays impinge on a scintillating material, the interaction causes electrons to be excited. De-excitation occurs with fluorescent radiation at a larger wavelength. This reaction takes place in a time interval (decay time) characteristic of the particular material. This scintillation radiation is received and amplified by a photomultiplier tube. For the particular device described above, the frontal and annulus crystal are operated in anti-coincidence with the central NaI(Tl). The difference between NaI and CsI decay times (1/4 and 1 μ sec respectively) allows the rear phoswitch crystal to be operated in anti-coincidence with the main

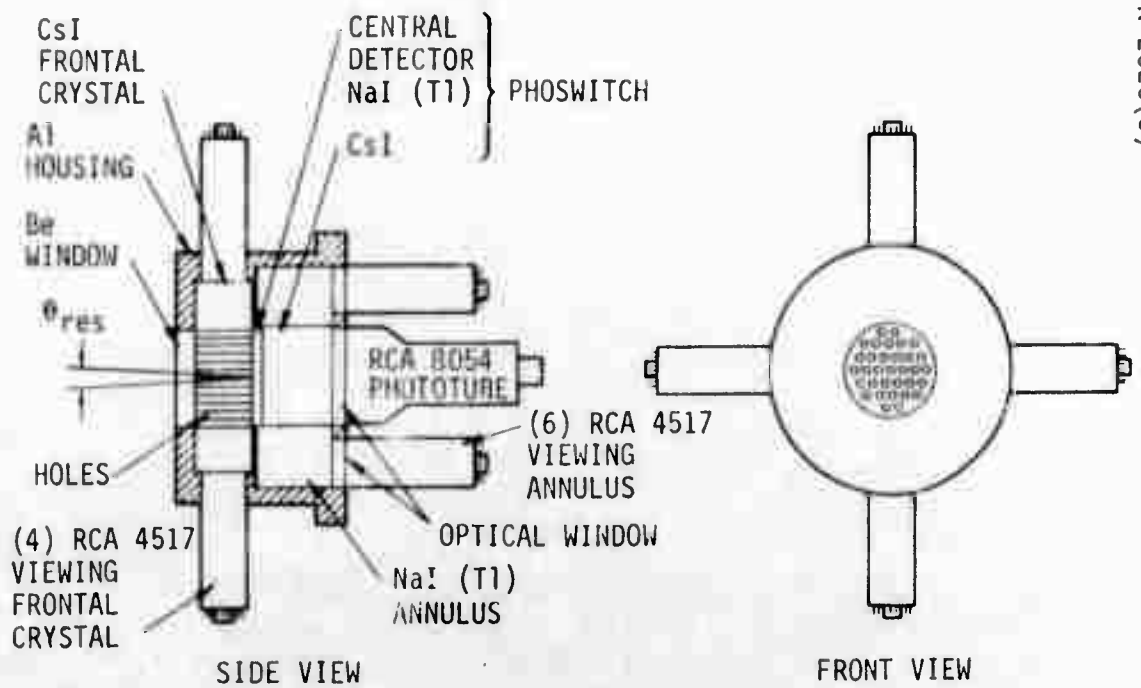

Figure 5-1(U). Scintillation Detector Similar to that Used by Hurley [24] to Search for X-Rays from Jupiter

crystal. An anti-coincidence signal enforces a mandatory dead time in sensing the central crystal for typically 200 μ sec. The effect of this anti-coincidence is, in intent, to only count X-rays which pass through the holes in the frontal crystal, and thus define a steradian of view and a view direction.

The outer crystals are referred to as active shielding as opposed to inactive shielding such as a lead shield. This active shielding serves to negate background counting of cosmic ray shower generated γ-rays. A passive shield alone would probably cause more background than it shields out.

The thickness and composition of the front window determines the minimum energy radiation viewed, while the thickness and composition of the main crystal determines the high energy limit of observed signals. These factors contribute to the efficiency of the detector

$$\varepsilon(E) = \exp\left(-t_w \mu_w(E)\right)\left|1 - \exp\left(-t_{cc}\mu_{cc}(E)\right)\right| \qquad (29)$$

which follows from Beer's law, with t_w and t_{cc} being the thicknesses of the window and central crystal, respectively, and $\mu_w(E)$ and $\mu_{cc}(E)$ being the absorption coefficients of the window and central crystal, respectively, as a function of photon energy. This equation assumes that all photons are detectable if they interact with the main crystal, which is a good approximation. In effect, this efficiency limits the "bandwidth" of the receiver. Further structuring of the bandwidth can be achieved through pulse height analysis, which discriminates energy of an X-ray counted to within a particular "energy bin" based on the shape of the signal output by the photomultiplier tube viewing the main crystal. This pulse height analysis allows the weighing of different "energy bins" and, therefore, tailoring or altering the efficiency. Background rejection techniques based on pulse height analysis are an example of this technique.

The angular resolution is defined by the thickness of the frontal crystal and the radius of the holes. If the radius of the hole is r_H, and length is t_F and N_H is the number of holes then

$$\theta_{res} \cong \frac{2r_H}{t_F} \tag{30}$$

and the effective collection area of the receiver is $A_R = \pi N_H r_H^2$. Typical devices used in experiments have had $N_H \lesssim 100$, $A_R \lesssim 100$ cm^2 which is approximately half the area of the window, $r_H \gtrsim 0.25$ cm and $t_F \lesssim 25$ cm. The smallest θ_{res} are typically a few degrees. Fragility of the crystals precludes smaller hole diameters. Larger N_H and greater thickness t_W are constrained ultimately by how large a crystal can be grown; however, finer resolution holes may be achievable by growing crystals around taut piano wire.

Total reflection of X-rays places a limit on achievable resolution because reflection from the side of the hole is not desired. A simple calculation yields (for CsI frontal crystal)

$$\theta_{res} \geq 3.2 \left(\frac{\lambda}{\text{Å}}\right) \times 10^{-3} \text{ radians} \tag{31}$$

for X-rays of wavelength λ. This limit is typically an order of magnitude below any devised apparatus to date.

At high energies X-rays may penetrate the active shielding (not through the holes) without registering an anti-coincidence signal and then scatter in the main detector to cause some background counting. It is usually argued [13] that if the average thickness $\bar{t}$ of the active shield is chosen so that leaked flux at the largest energy E_L of interest is on the order of the collimated flux, then this background will be no larger than the signal, i.e.,

$$\frac{\Omega_{res}}{4\pi} \cong e^{-t\mu(E_L)} \tag{32}$$

where Ω_{res} is the resolution steradian

$$\Omega_{res} \cong \pi\theta^2_{res} \tag{33}$$

and $\mu(E_L)$ is the absorption coefficient of the active shielding. A Monte Carlo [13] code has been used to predict this so-called "true detector background", but its success is still in doubt and the procedure has never been published. Another source of background counting is induced radioactivity in the shield due to very high energy cosmic rays and their spallation products. If this is the case, then there exists a thickness $\bar{t}$ of shielding beyond which the true detector background will increase, unlike the argument of Peterson [13] which implies that background goes to zero as $\bar{t}$ gets large. This situation is indicative of the lack of understanding of the causes for true detector background. In fact, all X-ray astronomy observations probably spend more time looking away from an object of investigation in order to obtain background levels than they spend collecting radiation from the object.

It should be noted that there is another significant collimating method used in X-ray astronomy measurements called modulation collimator. Invented by Oda [25] it consists of layers of wires in such a manner that the wires absorb incident photons if not coming from the correct steradian. It is like a number of picket fences in parallel. Achievable resolutions [26] are orders of magnitude greater than the device described above. However, they have only been used in conjunction with proportional counters (low energy), and it is not clear whether at higher energies the wire will significantly absorb the X-rays and also not yield at the same time high levels of true detector background. Another variation on Oda's invention

is a rotating modulation collimator [22]. If high energy modulation collimators are developed, they could be significant in reducing background counts which depend on steradian of view, such as the diffuse background, earth shine, and "space noise." In this case, true detector background which does not depend on field-of-view will probably dominate the background.

6. COUNTING STATISTICS

Based on the parameters defining the components and geometry of the X-ray discrimination system, there will be recorded at the receiver a mixture of the various background plus signal counts. Through the analysis of these photon counts, a determination of whether there was a target in the field-of-view must be made. In order to do this, we must examine the statistical properties of the background and signal.

Since photons produced by radioactive decay and by scattering are events which occur with probability proportional to time for small time intervals, the statistics which govern the counting rate are of the Poisson type. That is, if the average counting rate of photons per unit time is R, then the probability of observing n photons in a time span T is

$$P_n = e^{-RT} \frac{(RT)^n}{n!} \quad . \tag{34}$$

The average number of counts in time T is $\langle n \rangle$ where

$$\langle n \rangle \equiv N \equiv \sum_{n=0}^{\infty} n e^{-RT} \frac{(RT)^n}{n!} = RT \tag{35}$$

and the variance $\sigma^2 = \langle n^2 \rangle - \langle n \rangle^2$ is

$$\sigma^2 \equiv \sum_{n=0}^{\infty} n^2 e^{-RT} \frac{(RT)^n}{n!} - (RT)^2 = RT \quad . \tag{36}$$

Denoting by subscripts S and B the signal and background, it is easily shown that

$$N_S = R_S T$$

$$N_B = R_B T$$

$$N_{S+B} = T(R_S + R_B) = N_S + N_B \tag{37}$$

$$\sigma^2_{S+B} = \langle n^2_{S+B} \rangle - \langle n_{S+B} \rangle^2 = \langle (n_S + n_B)^2 \rangle - (\langle n_S \rangle + \langle n_B \rangle)^2$$

$$= \sigma_S{}^2 + \sigma_B{}^2 + 2 \left[\langle n_S n_B \rangle - \langle n_S \rangle \langle n_B \rangle \right] .$$

In the case where there is negligible correlation between background and signal, this last expression becomes

$$\sigma^2_{S+B} = \sigma_S{}^2 + \sigma_B{}^2 = N_S + N_B = N_{S+B} . \tag{38}$$

We will assume this to be the case, even though "space noise" is correlated to the signal. Let n^* be the number of counts received in a time T which we will consider indicative of a signal being present (i.e., a threshold value). We choose n^* to be at least P_o standard deviations less than the average number of counts for signal plus background, i.e.,

$$n^* \leq N_{S+B} - P_o \sqrt{N_{S+B}} \tag{39}$$

in order to have a P_o "sigma" confidence in seeing the signal if it is there. We further restrict n^* to be P_{fa} standard deviations greater than the average background when no signal is present

$$n^* > N_B + P_{fa} \sqrt{N_B} \tag{40}$$

so that we have a P_{fa} "sigma" confidence of no false alarm. In the limit that the number of counts gets large, the Poisson distribution can be approximated by a Gaussian distribution. For a Gaussian distribution, 1 "sigma" confidence corresponds to a probability of 0.841 and 2 "sigma" confidence to a probability of 0.977. We will, in general, use $P_{fa} = P_o = 2$.

Combining these relations we obtain

$$P_{fa} \sqrt{N_B} \leq N_S - P_o \sqrt{N_S + N_B} \quad . \tag{41}$$

Our instrument will intercept a certain flux of signal and background per unit area per unit time. Let these fluxes be I_S and I_B, then

$$I_S = \frac{R_S}{A_R} = \frac{N_S}{A_R T_R} \text{ and } I_B = \frac{R_B}{A_R} = \frac{N_B}{A_R T_R} \tag{42}$$

where A_R is the effective receiver area and T_R is the instrument view time. Expression (41) becomes

$$I_S \geq \sqrt{\frac{I_B}{A_R T_R}} \left[P_{fa} + P_o \sqrt{1 + \left(\frac{I_S}{I_B} \right)} \right] \quad . \tag{43}$$

Historically, in most cases of a developing system the signal will be weak compared to background and we have

$$I_S \geq \sqrt{\frac{I_B}{A_R T_R}} \left[P_{fa} + P_o \right] \quad \text{(weak signal)} \tag{44}$$

the opposite limit $I_S/I_B \gg 1$ yields

$$I_S \geq \frac{P_o^2}{A_R T_R} \quad \text{(strong signal).} \tag{45}$$

We will in general consider only the weak signal case. Since $\sqrt{I_B}$ is usually referred to as noise (i.e., jitter in background), Expression (44) can be interpreted in terms of signal-to-noise ratio S/N as

$$\left(\frac{S}{N}\right) \geq \left(P_{fa} + P_o\right) \Big/ \sqrt{A_R T_R} \quad . \tag{46}$$

Alternatively, these expressions can be used to indicate the value of $A_R T_R$ required to detect a given signal I_S when a background level I_B is present, i.e.,

$$A_R T_R \geq \frac{I_B}{I_S^2}\left[P_{fa} + P_o\sqrt{1+\left(\frac{I_S}{I_B}\right)}\right]^2 \tag{47}$$

$$\geq \left(P_{fa} + P_o\right)^2 \left(\frac{I_B}{I_S^2}\right) = \left(P_{fa} + P_o\right)^2 \left(\frac{S}{N}\right)^{-2} \quad \text{(weak signal)}$$

which indicates that maximizing signal-to-noise ratio minimizes required $A_R T_R$ to "see" the signal (in the weak signal limit).

The background intensity I_B is composed of "space noise," earth shine and diffuse background all dependent on the field-of-view Ω_{res} and the effective collection area of the receiver. The final component of I_B is the "true" detector background which is a function of the environment and design of the receiver and is independent of field-of-view. The total background is obtained by integrating over energy the product of the appropriate fluxes with the efficiency of the receiver. I_S is similarly obtained.

If the total background spectrum and signal spectrum have a variable signal-to-noise ratio as a function of energy, then the sensitivity of the receiver can be improved over that indicated above through different weighting of

pulse height analysis "energy bins." This technique in effect is an electronic-matched filter approach, and to date has not been used in X-ray astronomy. The only present use of this sort of technique is in the rejection of certain noise pulses based on their general signal shape.

Denoting the true detector background spectrum as $d^2N_{TB}/dEdA$ in photons per sec per unit energy per unit receiving area and the receiving steradian dependent background as $d^3N_{\Omega B}/d\Omega dEdA$ in photons per sec per unit energy per unit receiving area per receiving steradian, then the total background spectrum received is

$$\frac{dN_B}{dE} = A_R \left[\Omega_{res} \frac{d^3N_{\Omega B}}{d\Omega dEdA} + \frac{d^2N_{TB}}{dEdA} \right] . \tag{48}$$

Assuming the receiver has the target in its field-of-view, the signal spectrum seen will be

$$\frac{dN_s}{dE} = \frac{A_R}{R_R^2} \left[\frac{d^2N}{dEd\Omega} \right]_{\substack{\text{toward} \\ \text{receiver}}} . \tag{49}$$

The actual detected photons will be the above spectrum folded into the efficiency of the detector, i.e.,

$$\left.\begin{aligned} I_B A_R &= \int \varepsilon(E) \left(\frac{dN_B}{dE} \right) dE \\ \text{and} \qquad I_S A_R &= \int \varepsilon(E) \left(\frac{dN_s}{dE} \right) dE \ . \end{aligned}\right\} \tag{50}$$

In effect the efficiency limits the bandwidth of the receiver, and it will be the variability of this with the parameter t_w and t_{cc} which will allow us to optimize our ability to detect the signal over the camouflaging effect of background noise.

7. SYSTEM SYNTHESIS

In the previous sections, we have described the many varied aspects and components of an X-ray sensing system. The system as a whole should now be designed, but our ability to carry out this design is seriously constrained by the lack of knowledge of true detector background dependence on receiver construction and environment. There are also constraints such as weight, volume, and data transmission rates (etc.) which have been ignored in this preliminary analysis but which will restrict and alter any optimization of the eystem. We will give, therefore, only a broad general discussion of the synthesis which would have to be performed in constructing such a system.

1. Fix design of threat (target); such as Table 4-1.
2. Based on threat, choose type of detector system platforms and thus distances and time constraints.
3. Choose electron beam energy E_{elec} to be considered.
4. Description of X-ray transmitter.
   a. Current $i = i\ (E_{elec})$ from state-of-the-art curve (Figure 2-1)
   b. Assume an electron beam target of Z = 74, i.e., tungsten
   c. Efficiency $\eta = \eta\ (E_{elec})$ Expression (9)
   d. Gain in direction of target $G = G\ (E_{elec})$ Figure 2-2
   e. Transmitted X-ray spectrum per second per unit energy per steradian in direction of target

$$\frac{d^2N}{dEd\Omega} \text{ from Expression (10)}$$

5. Target scattering:
   a. From chemical composition determines the absorption coefficient as a function of energy

b. From geometry of system we have R_T and A_T and angle θ subtended at target by the receiver and transmitter

c. With an albedo-type calculation, determine $S = S(\theta,E)$

d. The scattered spectrum per unit energy per sec per steradian in the direction of the target is then

$$\left(\frac{d^2N}{dEd\Omega}\right)_{\substack{\text{toward}\\ \text{receiver}}} = \left[S(\theta,\ E')\ \frac{A_T}{R_T^2}\ \frac{d^2N}{dE'd\Omega}\ \left(\frac{E'}{E}\right)^2\right]_{E'=\frac{E}{\left[1-\frac{E}{E_C}(1+\cos\theta)\right]}} \tag{51}$$

6. X-ray receiver:

a. Geometry = $>R_R$

b. Parameters of receiver to be chosen optimally:

(1) Instrument window thickness t_w to limit low energy reception

(2) Frontal crystal thickness which we will assume is characteristic of the average active shield thickness $\bar{t}$. This would be chosen to reduce "true detector background to acceptable levels" (if physically possible), under constraints of weight, size, etc.

(3) Central crystal thickness t_{cc} chosen to limit high energy reception

(4) The resolution half angle θ_{res} will be chosen small enough to allow only minimal angular dependent background counts. Fragility constraints on crystal drilling

c. Efficiency $\varepsilon(E)$ of receiver: Expression (29)

d. Detected signal I_S and background I_B typically Expressions (51), (14), (12)

e. Receiver parameter $A_R T_R$ Expression (47). (T_R = receiver view time)

f. Return to Item 6(b) and interate until $A_R T_R$ minimal (i.e., find values for parameter in Item 6(b) which minimize $A_R T_R$)

7. Optimal system: Return to Item 3 and iterate E_{elec} until we find energy E_{elec} which produces the minimal of all minimal $A_R T_R$.

As mentioned above, understanding of true detector background is very limited and a full optimization is not possible. We will, however, perform an approximate analysis for what we will call an X-ray "probe" system.

Assume that we wish to have the X-ray sensor act as a direction finder for an object as "bright" as described by the straight line curve fits to the RV albedo in Figure 4-1. Because we will eventually wish to use the system to discriminate RV from RD we will use threat parameters from Table 4-1.

We assume the X-ray transmitter and receiver are on the same platform consisting of a Spartan-like missile, launched on warning to intercept and guide along the centerline of the threat tube (in opposite direction to threat) at threat apogee. Interception near threat apogee is necessitated by the MCD constraint of only a few interceptor farms. We further assume that there is an IR sensor (or other high resolution sensor) which searches for objects (RV's and RD's) to be investigated and queues the X-ray transmitter and receiver where to point. This queuing device frees the X-ray receiver from searching and thereby reduces the necessary photon flux for detection in a fixed time allowance. Moreover, there will have to be a range-finding device to provide knowledge of R_R (= R_T) necessary for comparative analysis of signals from different targets.

Based on the cross and in trajectory velocities imparted to RV and RD and the time to apogee (Table 3-1), we assume the threats to be distributed uniformly over a cylinder of radius $r_t = 4.9 \times 10^4$ ft and length $l_t = 3.9 \times 10^5$ ft. Since the probe traverses the axis but in opposite direction to the threats, we will assume a relative velocity of encounter of twice the threat velocity or $\sim 4 \times 10^4$ ft/sec. At this velocity the threat tube will be traversed in ~ 10 sec which allows about 1 sec of view time by the X-ray receiver per object based on assuming 1 RV and 12 RD's per booster (Table 4-1).

Due to dilution of received power with the fourth power of the distance, those objects on the threat cylinder surface at $R_T = R_D \cong 5 \times 10^4$ ft will stress the sensor system most. Moreover, since this distance is under the control of the offense, we must require the sensor system to work at least at this distance. For this reason, we will only be concerned with this characteristic target distance.

Due to lack of knowledge of true detector background, we will totally neglect it, even though it may dominate the background. We will assume only background counts from the diffuse cosmic component and space noise. Neglect of earth shine is reasonable since if looking at earth the background spectrum is similar to the diffuse spectrum (see Figure 3-7).

In order to obtain the space noise flux we must integrate Expression (12) over that volume of space for which the receiver beam cone and the transmitter beam cone intersect. To get a ball park estimate, we assume that the reciever steradian cone is about the same size as the sending cone and that the intersection will be approximated as a cone with an apex at a distance r_{min} from the receiver and subtending a steradian equal to the receiver steradian Ω_{rec}. Assuming the receiver and transmitter are separated by a distance D, then

$$r_{min} \cong \frac{D}{2\theta_{res}} \quad . \tag{52}$$

Into Expression (12) substitute

$$J = \frac{d^2N}{dEd\Omega}\left(\frac{1}{r^2}\right)$$

$$dV = r^2\ \Omega_{rec}\ dr$$

$$d\Omega = A_R/r^2$$

$$\text{and } \frac{d\sigma_c}{d\Omega} \cong \frac{\sigma_c}{4\pi}$$

then integrate from $r = r_{min}$ to ∞ and we obtain

$$\frac{\left(\frac{1}{A_R}\frac{dN}{dE}\right)_{\substack{\text{space noise}\\ \text{on receiver}}}}{\left(\frac{1}{A_R}\frac{dN}{dE}\right)_{\substack{\text{signal}\\ \text{on receiver}}}} \cong \frac{R_T^4 \rho_e \sigma_c \Omega_{res}}{4\pi\ S\ A_T\ r_{min}} \quad . \tag{53}$$

In actual fact σ_c is a function of energy similar to S(E) due to de-enhanced backscatter at high energy, and we will approximate $\sigma_c/4\pi S$ by σ_o which is the Thomson cross section (0.666 Barns). Thus,

$$\frac{I_{\text{space noise}}}{I_S} \cong \frac{2\pi\ R_T^4\ \rho_e \sigma_o \theta^3_{res}}{A_T D} \quad . \tag{54}$$

As the angular resolution we will assume

$$\theta_{res} = 0.005 \text{ radians} \tag{55}$$

which is typically an order of magnitude better than present X-ray astronomy sensors but does not violate Expression (31) for energies of interest.

In the backscatter case, the largest energy of interest will be 0.511/2 MeV since no Compton scattered photon will have energy greater than this. If we denote by E_{max} the maximum energy of a scattered photon at the receiver after Compton scattering, i.e.,

$$E_{max} = \frac{E_{elec}}{1 + \frac{2E_{elec}}{E_c}} \tag{56}$$

and denote by E_{min} the minimum energy counted at the receiver, then we will assume an efficiency

$$\varepsilon(E) = \left\{ \begin{array}{ll} 1 & \text{if } E_{max} \geq E \geq E_{min} \\ 0 & \text{otherwise} \end{array} \right\} . \tag{57}$$

This is a reasonable approximation for the continuous rise and fall of ε due to window thickness t_w and central crystal thickness t_{cc}.

With this very simple model, we can for any given energy E_{elec} find that value of E_{min} for which $A_R T_R$ is optimal. In Figure 7-1 we show the results for this probe X-ray sensor geometry. (We have assumed $\rho_e \simeq 3 \times 10^{10}/cm^3$ consistent with an altitude of $\sim$ 150 km.) As seen from this figure the space noise is a negligible component if I_B. Also note that $I_S/I_B << 1$ and we are, therefore, in the weak signal limit. The optimal $A_R T_R \cong 2.5 \times 10^7$ cm^2 sec occurs for a transmitter with beam energy $\sim$ 4 MeV. With a time constraint $T_R \sim 1$ sec, this implies a receiver collection area of 2.5×10^7 cm^2 which is typically 10^5 greater than scintillation detector X-ray telescopes at our energy ranges used in X-ray astronomy.

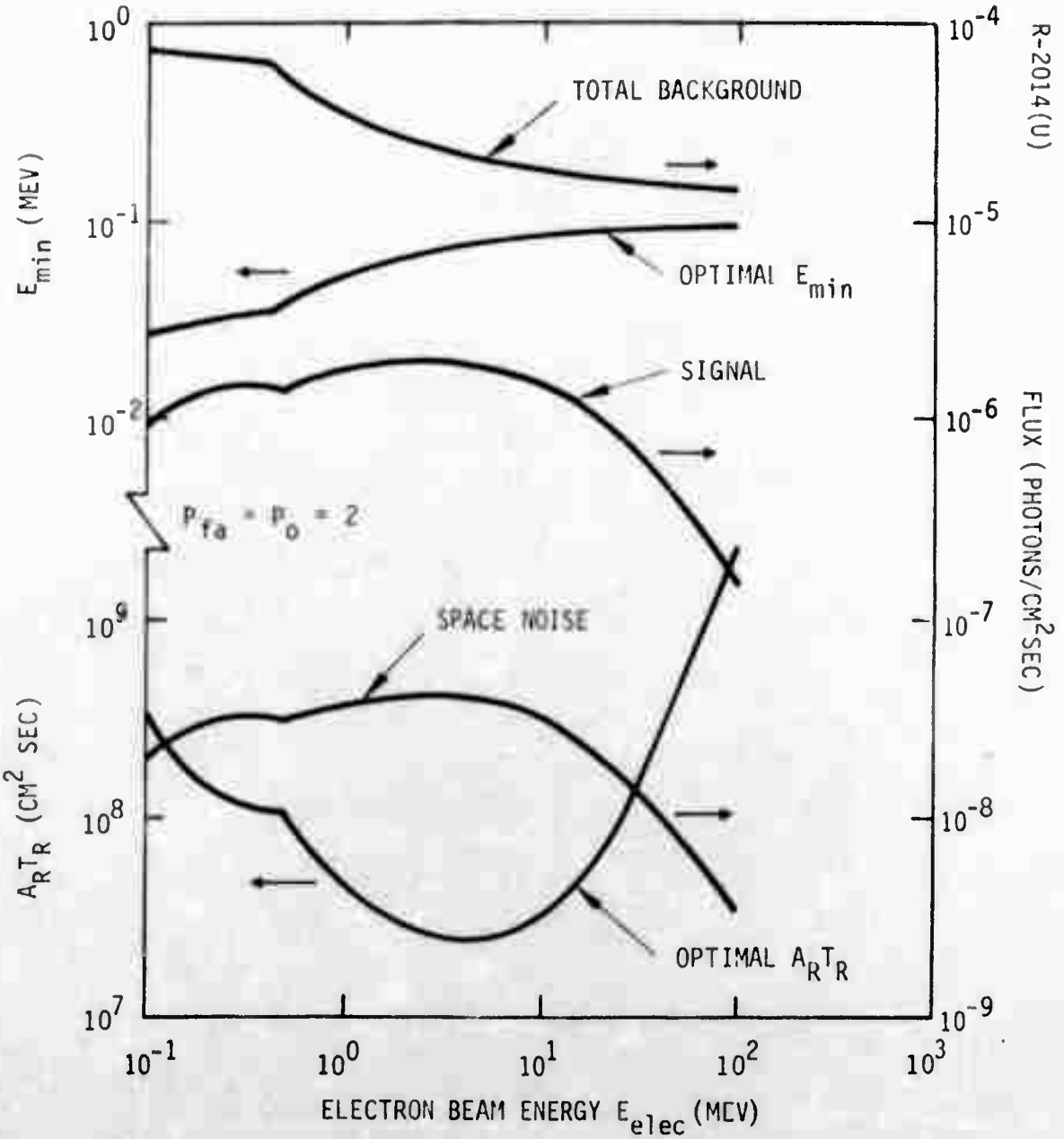

Figure 7-1(U). Optimal Receiver Collection Characteristics

The $A_R T_R$ curve in Figure 7-1 can be generalized considerably in the weak signal limit. By means of Expression (47) we can conclude:

1. Neglecting space noise, an increase α in θ_{res} will increase the background I_B by α^2 and thus increase $A_R T_R$ by α^2.
2. An increase in electron current of the X-ray generator by α over the state-of-the-art curve at fixed E_{elec} will increase the signal I_S by α and, therefore, decrease $A_R T_R$ by α^2. We note that if X-ray generators produce significantly more current, then space noise may be an important contributor to background. Furthermore, if $\alpha = \alpha(E)$ then the optimal X-ray transmitter energy E_{elec} may shift.

An alternative set-up can be envisioned where a series of X-ray transmitters and receivers are aboard a number of satellites; however, this approach is even less feasible than the probe set-up. We can define a "best" system geometry as one which requires the least value for reception area A_R. Since $A_R \sim I_S^{-2} T_R^{-1}$ in the weak signal case (or $A_R \sim I_S^{-1} T_R^{-1}$ in the strong signal case) and I_S is diluted with the fourth power of distance, i.e., $I_S \sim R^{-4}$, we can construct a geometry figure of merit $R^{-8} T_R$ in the weak signal limit (or $\sim R^{-4} T_R$ in the strong signal case). With this figure of merit concept, it is apparent that the probe geometry ($R \sim 9$ miles, $T_R = 1$ sec) is probably the best geometry possible. For example, it is very hard to visualize a system of satellites with an average standoff $R \sim 100$ miles, yet even if it existed and could view from launch to impact ($T_R \sim 2000$ sec), it cannot do better than the probe system.

8. ADVANTAGES OF A PULSED SYSTEM

After this research was concluded, it was realized that a pulsed X-ray system was far better and was not considered fully. Our typical X-ray generating devices (Figure 2-1) includes pulsed devices for beam energies above $\sim$ 1 MeV; however, we considered the receiver to be operating continuously. If we now allow the receiver to receive radiation only during the appropriate pulse reception times, we will receive the same average scattered signal flux, but we will reduce the effective background flux significantly. If f is the pulse repetition frequency, Δt is the pulse duration in time, and $\tilde{I}_B$ is the effective background flux then

$$\tilde{I}_B \cong I_B \, f\Delta t \text{ (provided } f\Delta t < 1) \; .$$

Typical values of f = 60 to 480 cps and $\Delta t = 10^{-3}$ to 10^{-6} sec thus correspond to orders of magnitude reduction in effective background levels. From Figure 7-1, we note the signal flux was about one order of magnitude below background flux; thus for typical pulsed systems, the signal flux will dominate effective background levels by at least one order of magnitude. When the signal is much stronger than the background, the criterion for seeing the signal is

$$A_R T_R > \frac{P_c^2}{I_s} \; .$$

A rough calculation for the probe geometry using source flux $\sim 10^{16}$ photons/steradian sec (from Figure 2-4), we obtain $A_R T_R \gtrsim 10^5$ cm^2 sec or about two orders of magnitude improvement over the continuous system (Figure 7-1). Moreover, since the background is small, the need for high resolution capability of the receiver is not as important for pulsed as it is for continuous operation.

Further information has come to our attention in relation to modern high current electron generators of the pulsed variety which are orders of magnitude better (in the average current sense) than our state-of-the-art curve (Figure 2-1). One example is the ASTRON device at the Lawrence Livermore Laboratory. It has the following characteristics:

$$\text{pulse repetition rate} = f = 60 \text{ cps}$$
$$\text{peak current} = i_p = 600 \text{ amps}$$
$$\text{pulse duration} = \Delta t = 0.3 \ \mu\text{sec}$$
$$\text{beam energy} = E_{elec} = 7\text{-}8 \text{ MeV}$$

The average current is $(i_p/2)\ f\Delta t \sim 5$ milliamp and is, thus, two orders of magnitude better technology than our state-of-the-art device at 7-8 MeV. Operating in a pulsed mode as described above, our X-ray device would require a receiver with $A_R \sim 10^5$ cm^2 and, thus, the ASTRON (with a target) would only require $A_R \sim 10^3$ cm^2; only one order of magnitude above present capabilities.

There are, however, two large drawbacks with high current machines.

1. The target used to stop the electrons would probably not withstand more than a few pulses before it would be destroyed.
2. These high current machines are physically big. For example, the ASTRON is over one hundred feet long and weighs many tons; obviously not appropriate for our probe sensor system.

9. METHODS OF INCREASING GAIN

We will discuss two possibilities for increasing the gain of the transmitter: the X-ray laser and X-ray optics.

9.1 X-RAY LASER

Of considerable interest in recent scientific literature is the claim by a group in Utah of having produced an X-ray laser [27]. The experiment has been doubted by a number of researchers mainly because very little information is contained in the original paper. One researcher has claimed the photographic evidence of X-rays was an accident of electrostatic discharge between photo film surfaces [28]; however, the experiment has been replicated [29] in such a manner as to refute this contention.*

A laser functions in the following manner: The electronic states of a lasing substance are raised (pumped) by chemical, thermal, or electromagnetic interaction. These excited electrons can decay with the resultant release of a photon in two ways: spontaneous decay and stimulated decay. Spontaneous decay is merely an incoherent process whereby the substance returns to a thermodynamic equilibrium condition. On the other hand, stimulated decay occurs when a photon of energy equal (or very near) to the decay energy interacts with the excited electron, and as a consequence induces the electron to decay and emit a photon. The emitted photon is emitted coherently with the perturbing photon (in phase and direction), and this physical process can, therefore, be looked at as an amplifier for that particular energy of photon, i.e., a laser. In order to increase amplification still further, most systems have an optical system (mirrors, prisms, etc.) which allow the beam being amplified to traverse the lasing substance many times before being "tapped" off for use.

---

*The authors of reference [29], however, have recently cast doubts on their own experiment: Applied Optics, Vol. 12, p. 1095.

For the Utah group's experiment, we can guess the following as occurring. The laser beam used to pump the $CuSO_4$ gel is focused by a cylindrical lense along a line in the gel. The interaction of this laser radiation with the matter at the focal line causes energy to be continually dumped into the gel substance thereby raising its temperature. If the energy can be dumped fast enough into the small volume of material near the focal line, then temperature ionization of the electrons will occur. Since this small volume is not in equilibrium with the rest of the gel substance, processes will ensue which attempt to establish equilibrium once more. These processes will include radiative emission of light and expansion of the heated substance into the cooler substance due to the imbalance of pressure. Then some atom's electron decoys spontaneously with a photon emitted along the focal line which is subsequently amplified by stimulated emission. Spurious "seed" photons occur in all directions but since in general the amplification is exponential in distance of lasing material traversed, only those photons along the focal line will undergo significant amplification. Since the lasing substance is a plasma, the pressure imbalance with the surrounding material makes this a destructive experiment.

It is simply impossible to attempt to scale the mentioned experiment into its future capabilities because of the lack of published information and because of the uncertainties in the various physical processes occurring. Some aspects of such a system, however, detract from its possible application as an X-ray transmitter.

1. Since the lasing substance is a plasma, the pressure imbalance with the surrounding material causes this to be a self-destructive experiment and, therefore, not convenient for rapid recycling or space applications. Confinement of this plasma by magnetic means does not seem to be a solution because present day confinement

densities are very low (and for short times), and since dumping of the laser (pumping) radiation will be proportional to density, the efficiency of pumping will decrease with density.

2. The attribute of phase coherence is of no use for the X-ray sensor system. Only directional coherence (i.e., gain or flux per steradian) is of consequence. Since at energies of interest, i.e., hard X-rays and weak γ-rays (based on Figure 4-1) there are no practical optical systems for X-rays, there is little hope for increasing gain by traversing the lasing substance more than once.

Information as to spectrum gain and efficiency, presently lacking, are needed at least to estimate potential and to compare with standard electron beam X-ray generators.

9.2 OPTICAL SYSTEMS FOR X-RAYS

The index of refraction n for X-rays is given approximately by the relation [30]

$$n = 1 - \delta$$

with

$$\delta = \frac{\rho_e e^2 \lambda^2}{2\pi m_e c^2} \quad \text{(ESU units)} \tag{58}$$

where ρ_e = electron density, e = electron charge, m_e = mass of electron and c = velocity of light. Since n is less than unity, X-rays are capable of being totally reflected by a polished surface of material for grazing

angles less than some critical angle θ_{crit} which by Snell's law is given as

$$\theta_{crit} = \sqrt{2\delta} \ . \tag{59}$$

This is predicated on the assumption that the X-ray energy is not too near an "absorption edge" of the material. (It is this critical angle which determined the constraint Expression (31) for CsI.) From Expressions (58) and (59) we note that θ_{crit} is proportional to wavelength and thus inversely proportional to energy of the X-ray photon.

A number of reflection optical systems have been designed for soft X-rays (typically less than 1 keV) consisting of parabolic and eliptical surfaces [22]. The purpose of these devices is to image objects usually on photographic film, the purpose being to see structure and to increase the signal-to-noise ratio by limiting the image to an area smaller than the collecting area.

For our X-ray sensor system we would want an optical system for different purposes depending on whether it is used with the receiver or transmitter. If used on the transmitter, its purpose would be to increase the gain (or power per steradian, i.e., partially collimate). Associated with the receiver the purpose would be to enhance the collection area to areas larger than constraints placed on scintillation crystal size, such as weight and possibly to define a better steradian resolution than the crystal is capable. In either case, we will have a slanted surface of material with characteristic dimensions $r_{\perp}$ and $r_{||}$ perpendicular and parallel to the viewing direction, such that $r_{\perp} \sim \theta_{crit}\, r_{||}$. Furthermore, we assume a cylindrical geometry about the viewing direction and a maximum radius of the reflecting material of R, see Figure 9-1.

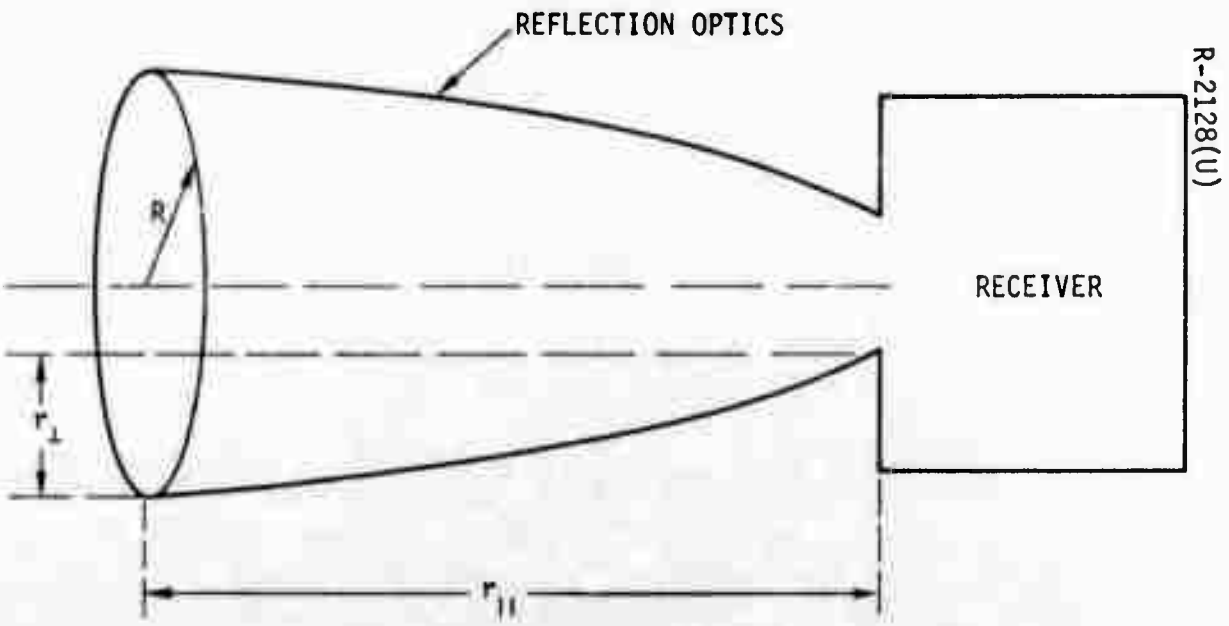

Figure 9-1(U). Conceptualization of Optical System

We can get an order of magnitude idea of dimensions of such collection and collimating systems by the following arguments: The collection area A_c for the receiver due to reflection optics will be on the order of

$$A_c \sim \pi \left[R^2 - (R - r_\perp)^2 \right] \sim \pi \left[R^2 - (R - \theta_{crit}\, r_{||})^2 \right] . \qquad (60)$$

Assuming crystal detectors could be built to achieve a collection area with effective radius $R_{crystal}$, and assuming the portion of the reflector at the receiver has a radius of this order, we could achieve a doubling of receiver collection area if

$$A_c \sim \pi R^2_{crystal} \sim \pi \left[R^2 - R^2_{crystal} \right]$$

and

$$R_{crystal} \sim R - \theta_{crit}\, r_{||}$$

or

$$R \sim \sqrt{2}\; R_{crystal}$$

and thus

$$r_{||} \sim \frac{\left(\sqrt{2} - 1\right) R_{crystal}}{\theta_{crit}} . \qquad (61)$$

Typical electron densities $\rho_e \sim 10^{25}/cm^3$ would yield from Expression (59)

$$\theta_{crit} \sim (10E/keV)^{-1} \text{ radians} \qquad (62)$$

and thus a probably achievable 3 inch value for $R_{crystal}$ implies $r_{||} \sim 1250$ inches at 100 keV.

In the transmitter application, analysis is not as easily estimated due to the fact that the electron beam focal point will be large to facilitate dissipation of heat in the tungsten target and thus the source of X-rays is not a point source. A parabolic type device will exactly collimate only those X-rays emanating from its focus point. A rough estimate is obtained as follows: Mentally abstracting Figure 9-1, let $\bar{r}$ be the mean distance from electron beam target material to the collimating optics. Moreover, let the area of the X-ray generating surface of the target material have a radius of r. The angle subtended at the mean optical system distance $\bar{r}$ by the edge of the X-ray generating surface is $\sim r/\bar{r}$. If, therefore, the central point of generation of X-rays is perfectly collimated, the outer portion will be diverging from the collimated direction by an angle $r/\bar{r}$. Since the optical system will subtend $\sim \theta_{crit}$ at the source of X-rays, the gain is

$$\left(\frac{\theta_{crit}}{(r/\bar{r})}\right)^2 \text{ or } \left(\frac{\bar{r}\theta_{crit}}{2}\right)^2 . \qquad (63)$$

This is very qualitative and must be taken with a grain of salt; however, it does have an intuitively satisfying form. The gain will increase in proportion to inverse (X-ray spot size)^2 and proportional to θ^2_{res}. Experimentally gains for spectroscopic energies (typically < 10 keV) have achieved 200 over isotropic [31]; however, extrapolating energy to 100 keV gives a factor of 2 in gain as possibly feasible.

In general, the conclusion is that at high energies, X-ray reflection optical systems become less and less effective in terms of collection or collimation. Moreover, the dimensions of such systems are awkward and cumbersome considering the minor increases in focusing they yield.

Due to the closensss of the index of refraction to one, transmission optics (i.e., lenses) can do nothing for X-rays since the X-rays are absorbed in thicknesses necessary to change beam direction.

10. SUMMARY AND RECOMMENDATIONS

The X-ray sensor system discussed in this report is in effect a means of remotely weighing an object. It is potentially a means of discriminating a replica decoy from an RV; however, X-ray generating capabilities and large area detector technology are presently too poor by orders of magnitude to make the system feasible against a MCD type threat.

We have tried to indicate the first-order considerations necessary in understanding and analyzing such a sensor. Because of the desire for simplicity, we have neglected or put little emphasis on many aspects including:

1. Characteristic atomic and nuclear transition radiation from the X-ray generator. Since these lines are typically very narrow, they offer a potential for increasing signal-to-noise by using much smaller bandwidth receivers.
2. Relativistically correct Bremsstrahlung spectrums and efficiencies.
3. True detector background.
4. Accurate modeling of the scattering by threat RV's and RD's.
5. Countermeasures such as the use of high Z materials on the RD could enhance the intermediate to high energy albedo due to larger number of electrons. Appropriate choice of florescent materials could cause humps in the albedo curve of the RD near florescent peaks. Both these CM's would, however, incur weight penalties on the defense.
6. Detector angular gimbaling rates for the probe case are on the order of 1 radian/sec, a fairly fast tracking rate.
7. Figure 2-1 is based on older references and may be considerably different today.

8. Non-backscatter sensor system could possibly achieve better scattered signal due to enhance forward Compton scattering at high energies; however, orchestration of the positions of transmitter and receiver could be very difficult.

As mentioned above, the X-ray sensor is presently unachievable in the context of a MCD threat. Since we have not considered other means of exo-discrimination, there is no reasonable way of judging whether the X-ray sensor is an effective path to pursue from a useful technology standpoint. However, noting the numerous applications made of sensors in other electromagnetic energy regions (i.e., photographic film, I-R sensors and imagers, radar, and radios), it would be prudent from an historical standpoint to pursue such a technology.

In the context of requirements for a system similar to that discussed, the avenues of research which could have the greatest impact are:

1. Research into X-ray devices with the sole goal of brute flux output and not subject to constraints of small electron beam focal points (typical for spectroscopic use) or phase coherency. This should include an analysis of the limits placed on X-ray outputs by the laws of physics and stability considerations subject to weight and volume constraints appropriate to space applications.
2. Research and experiments to further understanding and, therefore, predictability of true detector background as a function of environment and detector design parameter. The question of whether true detector background can be made as one wishes (except for thermal noise interior to the detector) should be answered.
3. Construction of modulation type collimators for energies in the 100 keV region and also construction of scintillation

crystals of angular resolution in the milli-radian range with reasonably good collection areas.

REFERENCES

1. W. Botch, F. Parry, A. Schaffer, S. Zeiberg, Light Area Defense Threat Final Report, R&D Associates, RDA-TR-156-ABMDA, 1973 (SRD).
2. Summary of Flights 1 to 5 of Replica Decoys, Lincoln Labs, PA 196, 1969 (SRD).
3. R. Berkowitz, ed., Modern Radar (John Wiley & Sons, Inc., New York, 1965).
4. R. McMaster, ed., Nondestructive Testing Handbook, Vol. 1, (Ronald Press Co., New York, 1959), Section 14.
5. G. Clark, Applied X-Rays, (McGraw - Hill Book Co., Inc., New York, 1955).
6. S. Flugge, ed., Handbuch Der Physik, Vol. XXX, (Springer - Verlag, Berlin, 1957); S. Stephenson, "The Continuous X-Ray Spectrum", p. 337.
7. E. Condon, H. Odishaw, eds., Handbook of Physics (McGraw - Hill Book Co., Inc., New York, 1958); E. Condon, "X-Rays", pp. 7-118.
8. Op. Cit., Clark, pp. 173, 174.
9. M. Livingston, J. Blewett, Particle Accelerators (McGraw - Hill Book Co., Inc., New York, 1962), p. 229.
10. Op. Cit., Flugge; W. Schaaffs, "Erzeugung von Rontgenstrahlen", p. 1.
11. R. Latter, R. LeLevier, Journal Geophysical Res., 68, 1643 (1963).
12. The Rocket Panel, Phys. Rev., 88, 1027 (1952)
13. L. Peterson, R. Pelling, J. Matteson, Space Science Reviews, 13, 320 (1972).
14. L. Gratton, ed., I. A. U. Symposium No. 37; Non-Solar X- and Gamma-Ray Astronomy (D. Reidel Publishing Co., Dordrecht, Holland, and Springer - Verlag Inc., New York, 1970); P. Agrawal, S. Biswas, G. Gokhale, V. Iyengar, P. Kunte, R. Manchanda, B. Sreekantan, p. 104.
15. Ibid.; L. Peterson, p. 59.
16. Ibid.; S. Ananthakrishnan, S. Chakravarty, K. Ramanathan, p. 146.
17. Ibid.; G. Clark, G. Garmire, W. Kraushaar, p. 269.
18. Ibid.; D. Brini, F. Fuligni, E. Horstman-Moretti, p. 321.
19. Private Communication; Skip Knowles (RDA).
20. W. Heitler, The Quantum Theory of Radiation (Oxford Univ. Press, London, 1954), p. 217 - .

21. D. Raso, M. Berger, Radiation Research, 12, 20 (1960).

22. F. Labuhn, R. Lust, eds., I. A. U. Symposium No. 41, New Techniques in Space Astronomy (D. Reidel Publishing Co., Dordrecht, Holland and Springer - Verlag New York Inc., New York, 1971), R. Giacconi, p. 104.

23. Ibid.; C. Fichtel, p. 15.

24. J. Hurley, Journ. Geophysical Research, 77, 46 (1972).

25. M. Oda, Applied Optics, 4, 143 (1965).

26. Ref. (14), M. Matsuoka, S. Miyomoto, J. Nishimura, M. Oda, Y. Ogawara, M. Wada, p. 130.

27. J. Kepros, E. Eyring, W. Cagle, Jr., Proc. Nat. Acad. Sci., USA, 69, 1744 (1972).

28. T. Boster, Applied Optics, 12, 433 (1973).

29. R. Elton, L. Palumbo, R. Andrews, R. Eckardt, J. Bradford, Applied Optics, 12, 155 (1973).

30. F. Richtmyer, E. Kennard, Introduction to Modern Physics, (McGraw-Hill Book Co., Inc., New York, 1947), p. 524

31. Op. Cit., Clark, p. 108.